

RESEARCH ARTICLE

FGF signaling promotes spreading of fat body precursors necessary for adult adipogenesis in *Drosophila*

Yuting Lei¹✉, Yuwei Huang¹✉, Ke Yang¹, Xueya Cao¹, Yuzhao Song¹, Enrique Martín-Blanco², José Carlos Pastor-Pareja^{1,3,4*}

1 School of Life Sciences, Tsinghua University, Beijing, China, **2** Instituto de Biología Molecular de Barcelona, Consejo Superior de Investigaciones Científicas, Parc Científic de Barcelona, Barcelona, Spain, **3** Tsinghua-Peking Center for Life Sciences, Beijing, China, **4** Institute of Neurosciences, Consejo Superior de Investigaciones Científicas-Universidad Miguel Hernández, San Juan de Alicante, Spain

✉ These authors contributed equally to this work.

* jose.pastorp@umh.es



OPEN ACCESS

Citation: Lei Y, Huang Y, Yang K, Cao X, Song Y, Martín-Blanco E, et al. (2023) FGF signaling promotes spreading of fat body precursors necessary for adult adipogenesis in *Drosophila*. PLoS Biol 21(3): e3002050. <https://doi.org/10.1371/journal.pbio.3002050>

Academic Editor: François Schweisguth, Institut Pasteur, FRANCE

Received: April 26, 2022

Accepted: February 24, 2023

Published: March 22, 2023

Copyright: © 2023 Lei et al. This is an open access article distributed under the terms of the [Creative Commons Attribution License](https://creativecommons.org/licenses/by/4.0/), which permits unrestricted use, distribution, and reproduction in any medium, provided the original author and source are credited.

Data Availability Statement: All relevant data are within the paper and its [Supporting information files](#).

Funding: This work was funded by grants 32150710524 and 91854207 from the National Natural Science Foundation of China (<https://nsfc.gov.cn>) and grant PID2021-122119NB-I00 from Ministerio de Ciencia e Innovación (<https://www.ciencia.gob.es>), all to J.C.P.-P. J.C.P.-P. was also funded by the “Severo Ochoa” Program for Centers of Excellence (CEX2021-001165-S) from Ministerio

Abstract

Knowledge of adipogenetic mechanisms is essential to understand and treat conditions affecting organismal metabolism and adipose tissue health. In *Drosophila*, mature adipose tissue (fat body) exists in larvae and adults. In contrast to the well-known development of the larval fat body from the embryonic mesoderm, adult adipogenesis has remained mysterious. Furthermore, conclusive proof of its physiological significance is lacking. Here, we show that the adult fat body originates from a pool of undifferentiated mesodermal precursors that migrate from the thorax into the abdomen during metamorphosis. Through in vivo imaging, we found that these precursors spread from the ventral midline and cover the inner surface of the abdomen in a process strikingly reminiscent of embryonic mesoderm migration, requiring fibroblast growth factor (FGF) signaling as well. FGF signaling guides migration dorsally and regulates adhesion to the substrate. After spreading is complete, precursor differentiation involves fat accumulation and cell fusion that produces mature binucleate and tetranucleate adipocytes. Finally, we show that flies where adult adipogenesis is impaired by knock down of FGF receptor Heartless or transcription factor Serpent display ectopic fat accumulation in oenocytes and decreased resistance to starvation. Our results reveal that adult adipogenesis occurs de novo during metamorphosis and demonstrate its crucial physiological role.

Introduction

Eukaryotic cells can efficiently store energy in the form of fat inside lipid droplets. Lipid droplets are ER outgrowths consisting of a core of neutral lipids surrounded by a phospholipid monolayer [1]. Many unicellular eukaryotes and certain cell types in multicellular ones possess the ability to produce lipid droplets. However, in the animal kingdom, both vertebrates and arthropods have concentrated lipid storage and release functions in large specialized cells called adipocytes. Differentiated adipocytes associate into adipose tissues and display giant

de Ciencia e Innovación. The funders had no role in study design, data collection and analysis, decision to publish, or preparation of the manuscript.

Competing interests: The authors have declared that no competing interests exist.

lipid droplets that occupy most of their cytoplasm. In vertebrates, histogenesis of adipose tissue (adipogenesis) is quite complex. Vertebrate adipocytes are generally believed to be of mesodermal origin, but specific populations have been found to derive instead from the neural crest [2]. In addition to fully differentiated adipocytes, mammalian adipose tissues contain stem cell precursors capable of producing new adipocytes [3,4]. Adipose tissue remodeling through formation of new adipocytes (hyperplasia) is a healthy response to caloric excess, whereas expansion of existing adipocytes through increased fat storage (hypertrophy) stresses those cells and associates with metabolic disease [5]. In contrast to adipocyte hyperplasia or hypertrophy, lipodystrophies are a group of congenital and acquired disorders characterized by the absence of functional adipocytes, causing insulin resistance, hyperlipidemia, and other metabolic complications [6]. Better knowledge of basic adipogenetic mechanisms, therefore, is essential to understand and treat conditions affecting adipose tissue health.

Besides vertebrates, the existence of true adipocytes and adipose tissue is documented in arthropods. The adipose tissue of arthropods, called fat body, has been extensively studied in insects, but is also present in crustaceans, chelicerates (spiders, scorpions, and mites), and myriapods [7]. Within insects, research in the fruit fly *Drosophila melanogaster* has described the presence of mature fat body in 2 stages of the life cycle of the animal: the larva and the adult. The development of the larval fat body, known to originate from the embryonic mesoderm, is well characterized. Shortly after gastrulation, different groups of mesodermal cells become specified within each segment to give rise to segmental populations of precursors for the somatic musculature, visceral musculature, heart mesoderm, gonadal mesoderm or fat body, depending on antero-posterior and dorso-ventral positional cues provided in part by the overlying ectoderm/epidermis to which they attach [8,9]. Precursors of the larval fat body, in particular, arise at lateral positions inside the domain of expression of segmentation gene *eve* [9,10]. The earliest sign of fat body differentiation is the expression at stage 10 of the transcription factor Serpent (Srp), required for fat body development [9,11,12]. During the larval stages, after segmental precursors have joined into a continuous larval adipose tissue, larval fat body adipocytes increase their cell size and ploidy through nutrition-dependent endoreplication [13]. Later, the larval fat body undergoes cell dissociation and histolysis during metamorphosis [14,15]. Isolated larval fat body cells are found inside the adult abdomen until 2 days after eclosion. However, in addition to the disappearing larval adipocytes, the eclosed adult displays segmental plates of adult fat body lining the abdomen (Fig 1A), with lesser amounts found in the head, thorax, and female gonads. In contrast to the well-known development of the larval fat body, adult fat body adipogenesis has remained mysterious to this date [16–18]. Clonal analysis shows that the adult fat body, like the larval fat body, is mesodermal in origin [19]. A possible relation between the larval and adult adipose tissues has been a matter of speculation and discussion for long time. Two alternative mechanisms for adult adipogenesis have been proposed: partial reassociation of the dissociated larval fat body [20] or de novo adipogenesis from undifferentiated precursors [21]. Many functional studies support a crucial involvement of the larval fat body in energy storage and metabolic regulation in the fast-feeding larva. Fewer studies, however, have tried to address the role of the adipose tissue in mature adult flies. Furthermore, due to insufficient knowledge of the development of the adult fat body and the lack of genetic tools to specifically image and manipulate it, conclusive proof of its physiological significance has been lacking.

In this study, we set out to investigate the development of the adult fat body in *Drosophila*. Through in vivo imaging, we found that the adult fat body originates from a pool of precursors that migrate from the thorax into the abdomen during metamorphosis. These precursors spread from the ventral midline in a process strikingly reminiscent of embryonic mesoderm migration, requiring fibroblast growth factor (FGF) signaling as well. In addition, we show

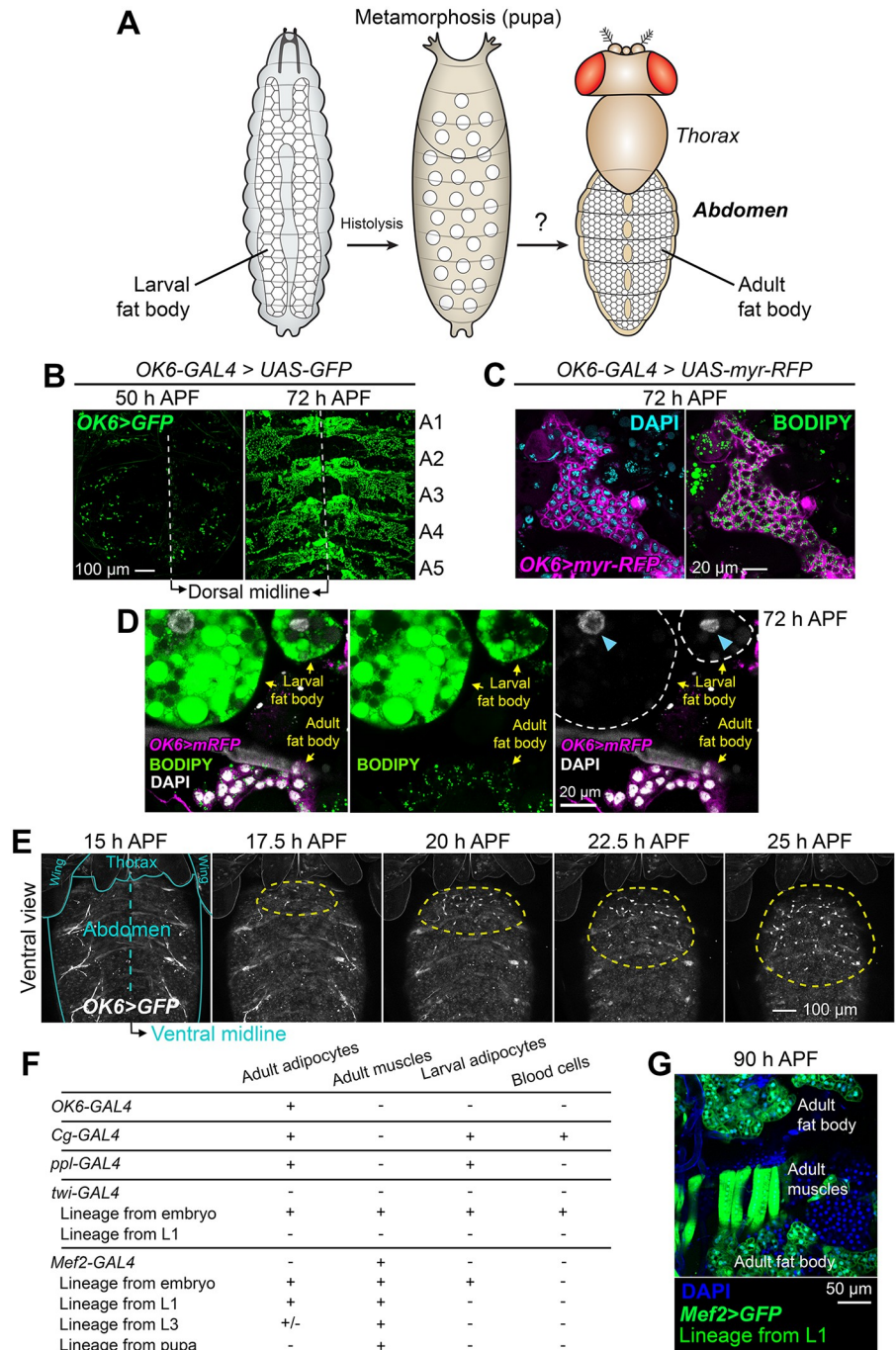


Fig 1. Adult fat body precursors migrate into the abdomen during metamorphosis. (A) Schematic cartoon depicting the adipose tissue (fat body) in *Drosophila* larvae and adults. The larval fat body, originating from embryonic mesoderm, disintegrates during metamorphosis. It is not known if the adult fat body is built from larval fat body remnants or assembled de novo from an alternate source of adipocytes. (B) Expression of GFP (green) driven by *OK6-GAL4* in pupal abdomens dissected and mounted flat at 50 and 72 h APF (after puparium formation). Abdominal segments A1 to A5 are indicated. (C) Adult fat body marked with *OK6-GAL4*-driven myr-RFP (magenta) at 72 h APF. Nuclei stained with DAPI (cyan, left) and neutral lipids with BODIPY (green, right). (D) Detail of a 72 h APF abdomen stained with BODIPY (green) showing together adult fat body (*OK6>myr-RFP*, magenta) and dissociated larval adipocytes. Note the large size of these highly polyploid cells and of their nuclei (blue arrowheads). (E) Still images from a time-lapse recording of an *OK6>GFP* pupa (ventral view). To image the ventral abdomen, legs were gently displaced anteriorly. Blue lines outline wings, thorax, and abdomen. Yellow dashed lines surround the growing population of *OK6*-positive cells migrating into the abdomen and proliferating there. Images are maximum intensity

projections of 61 confocal sections. See [S1 Video](#). (F) Summary of GAL4 expression patterns, indicating the presence (+) or absence (-) of GFP expression under control of *OK6-GAL4*, *Cg-GAL4*, *ppl-GAL4*, *twi-GAL4*, and *Mef2-GAL4* in different mesodermal derivatives. Shown as well are the results of lineage tracing experiments in which the progeny of all cells that express *twi-GAL4* or *Mef2-GAL4* at a given stage become permanently labeled (see [Methods](#)). (G) Abdomen of a pupa dissected 90 h APF in which cells that have expressed *Mef2-GAL4* up to the L1 stage are labeled with GFP (green). Summarized genotype: *Mef2-GAL4 + tub-GAL80^{ts} > UAS-Flp > act-y+> GAL4 > UAS-GFP*. Nuclei stained with DAPI (blue).

<https://doi.org/10.1371/journal.pbio.3002050.g001>

that flies in which adult fat body development is impaired display decreased resistance to starvation.

Results

Adult fat body precursors migrate into the abdomen during metamorphosis

Searching for tools that could help investigate the development of the adult fat body ([Fig 1A](#)), we came across *OK6-GAL4*, a GAL4 enhancer trap insertion in the second chromosome [22]. When we crossed *OK6-GAL4* to *UAS-GFP* flies, we observed expression of GFP in the pupal abdomen during metamorphosis. At 72 h APF (after puparium formation), *OK6*-driven GFP did not label the cells of the dissociated larval fat body, but was visible in segmental plates of tissue reminiscent of the morphology of the adult fat body ([Fig 1B](#)). Staining with the neutral lipid dye BODIPY showed that *OK6*-positive cells contained lipid droplets, consistent with their identity as developing adipocytes ([Fig 1C](#)). Furthermore, these *OK6*-positive cells were distinct from the dissociated larval adipocytes, which were larger and did not express *OK6-GAL4* ([Fig 1D](#)). Because at earlier stages of metamorphosis *OK6*-driven GFP was expressed in single cells attached to the abdominal epidermis, we hypothesized that these were the precursors of the adult fat body. Time-lapse imaging of the pupa (see [Materials and methods](#)) revealed that *OK6*-positive cells started arriving from the thorax at around 15 h APF, migrating and proliferating on the ventral epidermis of the abdomen ([Fig 1E](#) and [S1 Video](#)). To investigate the origin of these cells, we performed lineage tracing experiments. In these, GAL4-driven expression of the recombinase Flp, together with a flip-out cassette and thermosensitive GAL4 repressor GAL80^{ts}, labeled the progeny of cells expressing at a given stage *twi-GAL4* (embryonic mesoderm) and *Mef2-GAL4* (myoblasts and muscles) (see [Methods](#)). Lineage tracing with *twi-GAL4* in the embryo labeled adult adipocytes ([Fig 1F](#)), confirming their mesodermal origin [19]. Remarkably, *Mef2-GAL4* tracing in larva 1 (L1) stage labeled adult (but not larval) adipocytes and adult muscles ([Fig 1G](#)). This result shows that adult and larval adipocyte lineages have diverged at the L1 stage and additionally suggests that adult adipocytes and muscles may descend from a common larval population of progenitors. Altogether, our data show that the adult fat body derives from a population of undifferentiated mesodermal precursors that migrate from the thorax into the abdomen during metamorphosis.

The GATA transcription factor *Serpent* is required for early amplification of adult fat body precursors

Expression of the transcription factor *Serpent* (*Srp*) marks the precursors of the larval fat body in the embryo [11]. Furthermore, *srp* mutant embryos lack fat body, indicating that *Srp* is essential for correct development of the larval fat body [12]. We stained pupal abdomens with anti-*Srp* antibody and found that *Srp* was expressed in the adult fat body precursors, labeled with *OK6-GAL4*-driven GFP expression, and localized to their nuclei ([Fig 2A](#)), hinting an involvement of *Srp* in adult fat body formation as well. In order to test this, we knocked down

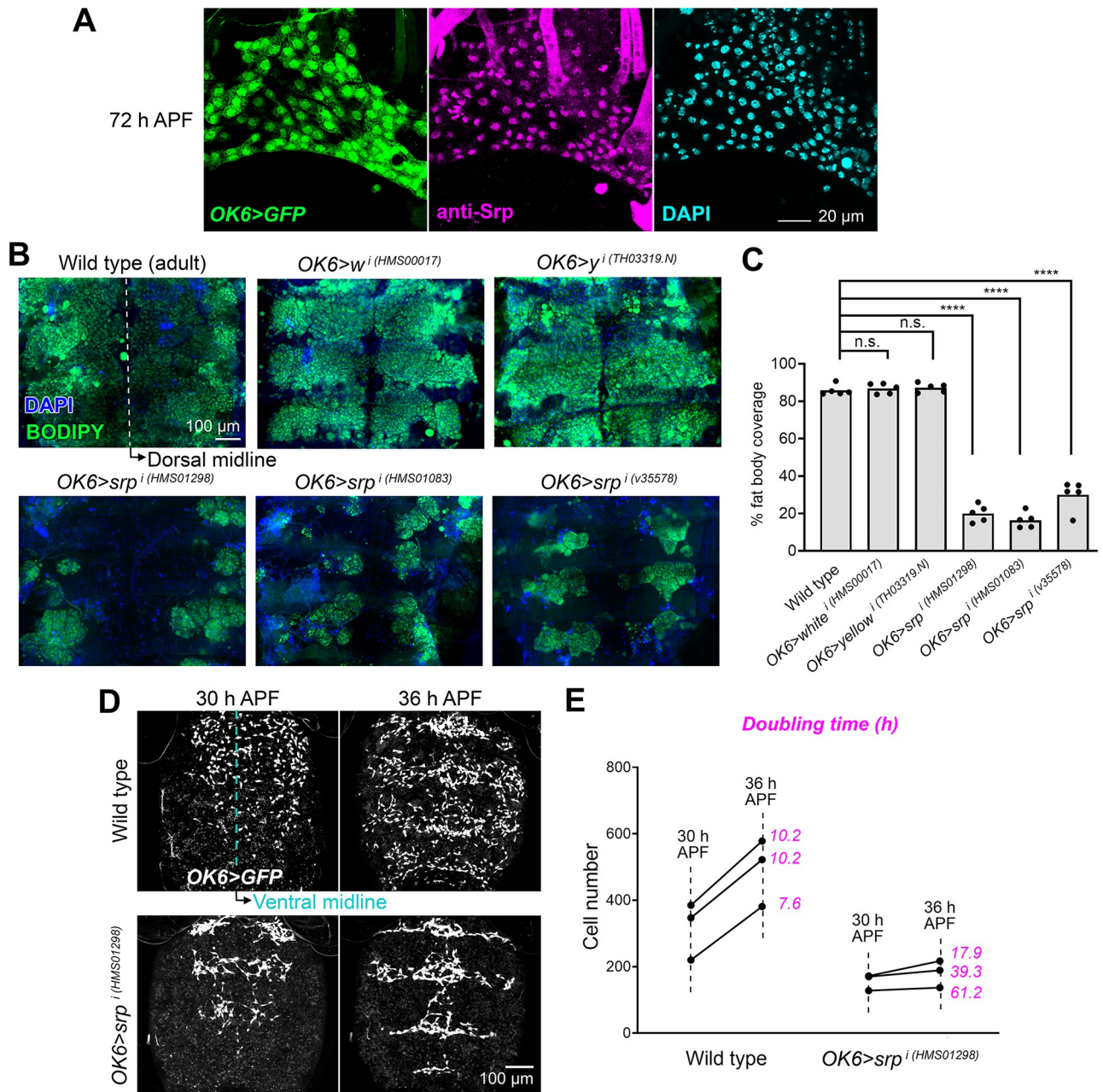


Fig 2. The GATA transcription factor Serpent is required for amplification of adult fat body precursors. (A) Adult fat body precursors (*OK6-GAL4*-driven GFP, green) from an abdomen dissected 72 h APF and stained with anti-Srp antibody (magenta). Nuclei stained with DAPI (cyan). (B) Adult abdomens from a wild-type fly and flies in which *srp* was knocked down with 3 different RNAi transgenes under *OK6-GAL4* control (*OK6>srpⁱ*). Controls knocking down genes *white* (*OK6>wⁱ*) and *yellow* (*OK6>yⁱ*) are shown as well. Abdomens were dissected 2 days after eclosion and mounted flat after staining with DAPI (nuclei, blue) and BODIPY (neutral lipids, green). (C) Quantification of adult fat body reduction upon *srp* knock down. Graph represents the coverage of adult fat body measured in images like those in (B) in at least 5 individuals per genotype, with the height of the bar indicating mean value. Significance of comparisons with the wild type in unpaired *t* tests reported as follows: n.s.: $p > 0.05$; ****: $p < 0.0001$. (D) Adult fat body precursors (*OK6-GAL4*-driven GFP, white) imaged in vivo in the abdomen (ventral view) of wild-type (top) and *OK6>srpⁱ* (bottom) pupae at 30 (left) and 36 (right) h APF. Images are maximum intensity projections of 65 confocal sections. (E) Graph representing number of adult fat body precursors at 30 and 36 h APF in 3 wild-type and 3 *OK6>srpⁱ* animals. Cells were counted in images like those in (D). The data underlying the graphs in the figure can be found in [S1 Data](#).

<https://doi.org/10.1371/journal.pbio.3002050.g002>

the expression of *srp* in the precursors of the adult fat body using *OK6-GAL4*-driven transgenic RNAi (S1A Fig). In the abdomen of both wild-type and *OK6>srpⁱ* adults dissected 2 days after eclosion, BODIPY staining revealed the presence of some fat body tissue. However, compared to wild-type, *OK6>wⁱ* and *OK6>yⁱ* control adults, the fat body of *OK6>srpⁱ* adults was severely reduced (Fig 2B and 2C). To investigate the genesis of this phenotype, we imaged the adult fat body precursors using *OK6-GAL4*-driven GFP expression. We found that precursors were present in the ventral abdomen of *OK6>srpⁱ* pupae at 30 h APF (Fig 2D). However, in contrast to the fast proliferation of these cells observed in the wild type, the number of precursors had increased less when we analyzed the same animal 6 h later at 36 h APF (Fig 2E). Counting of cell division events in live recordings lasting 6 h (S1B Fig and S2 Video) showed 132 mitosis/385 initial cells in wild type (0.342 mitosis/cell), and 29 mitosis/172 initial cells in *OK6>srpⁱ* (0.168 mitosis/cell), indicating a strong difference in proliferation rates. To additionally explore the contribution of apoptosis to the reduction of the adult fat body upon *srp* knock down, we performed TUNEL staining and found occasional apoptosis in *OK6>srpⁱ* precursors (S1E and S1F Fig). Because we never observed apoptosis in wild-type precursors, this result, while not statistically different from the wild type, led us to further test the effect of apoptosis. To do that, we expressed apoptosis inhibitor p35 while knocking down expression of *srp*. This, however, failed to rescue or modify *OK6>srpⁱ* adult fat body reduction (S1G and S1H Fig), suggesting that precursor apoptosis played a minor role in this reduction.

To further probe the role of Srp in adult fat body development, we used the Flp/FRT system to generate adipocyte precursors homozygous mutant for *srp⁰¹⁴⁵⁹*, an *srp* null mutant allele [23]. To do that, we drove expression of recombinase Flp in precursors under control of *OK6-GAL4* and assessed mitotic recombination in the FRT82B site by the loss of the marker Ub-GFP (Fig 3A). Control wild-type clones, negatively labeled by the lack of GFP, represented 42.8% ±3.6 SD of the fat body in pupal abdomens dissected 70 h APF, indicating high efficiency of clone induction (Fig 3B). Homozygous *srp⁰¹⁴⁵⁹* nuclei, in contrast, were 23.6% ±6.7 SD of the adult fat body nuclei at 70 h APF, evidencing a growth disadvantage of these cells. Nonetheless, mutant precursors seemed well integrated and displayed lipid droplets (S1I Fig). From these results, we conclude that Srp expression in adult fat body precursors is necessary for the amplification of their numbers during the early phases of adult adipogenesis. Our results additionally suggest that Srp may not be involved in their correct specification and differentiation into adipocytes.

Adult fat body precursors spread from the ventral midline

To further investigate adult adipogenesis, we recorded and analyzed the behavior of adult fat body precursors after the initial migration that brings them to the abdomen. Time-lapse imaging of *OK6>GFP* animals from 30 h APF showed that precursors in the ventral abdomen quickly converge towards the ventral midline at about 32 h APF (Fig 4A and S3 Video). This convergent movement is coincident with the time when the expanding nests of histoblasts (adult epidermal cells) push and replace the contracting ventral epidermis of the larva [24]. After this ventral contraction, adult fat body precursors spread on the abdominal epidermis, first laterally (Fig 4A and S3 Video) and then dorsally (Fig 4B and S3 Video), as they continue to increase their numbers through cell proliferation. Once the spreading precursors reach the dorsal side, they converge towards the dorsal midline from left and right (Fig 4C and S3 Video). Tracking of cell trajectories showed that adult fat body precursors experienced frequent changes of direction and repulsive interactions during their spreading when they contacted or collided with each other (Fig 4D and S3 Video). At the same time, analysis of the direction of migration with a 4-min resolution (the recording interval of our movies) revealed

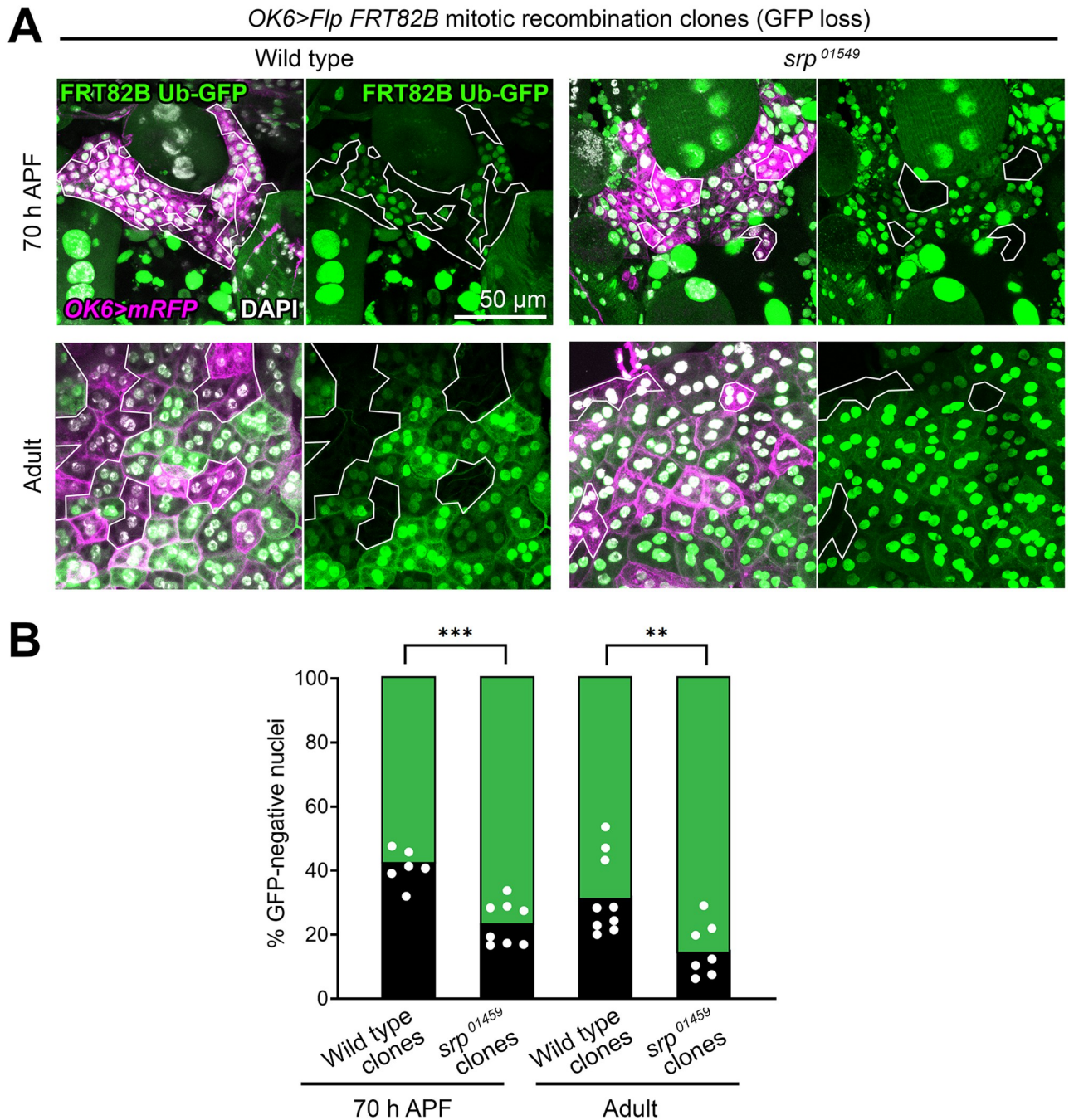


Fig 3. *srp* mutant clones are underrepresented in the adult fat body. (A) Adult fat body containing wild-type control (left) or *srp* mutant (right) mitotic recombination clones induced by expression of recombinase Flp under control of *OK6-GAL4*. Clones (outlined) are negatively labeled by the absence of Ub-GFP (green) in abdomens dissected at 70 h APF (upper row) or 2 days after eclosion (lower row). *OK6-GAL4*-driven myr-RFP in magenta. Nuclei stained with DAPI (white). (B) Graph representing the percentage of GFP-negative nuclei (wild-type control or *srp* mutant clones) in adult fat body dissected at 70 h APF or 2 days after eclosion. Each dot represents a measurement of that percentage in a different individual. The height of the black columns marks mean values. Differences between wild-type and mutant clones are significant in unpaired *t* tests. **: $0.01 > p > 0.001$; ***: $0.001 > p > 0.0001$. The data underlying the graphs in the figure can be found in [S1 Data](#).

<https://doi.org/10.1371/journal.pbio.3002050.g003>

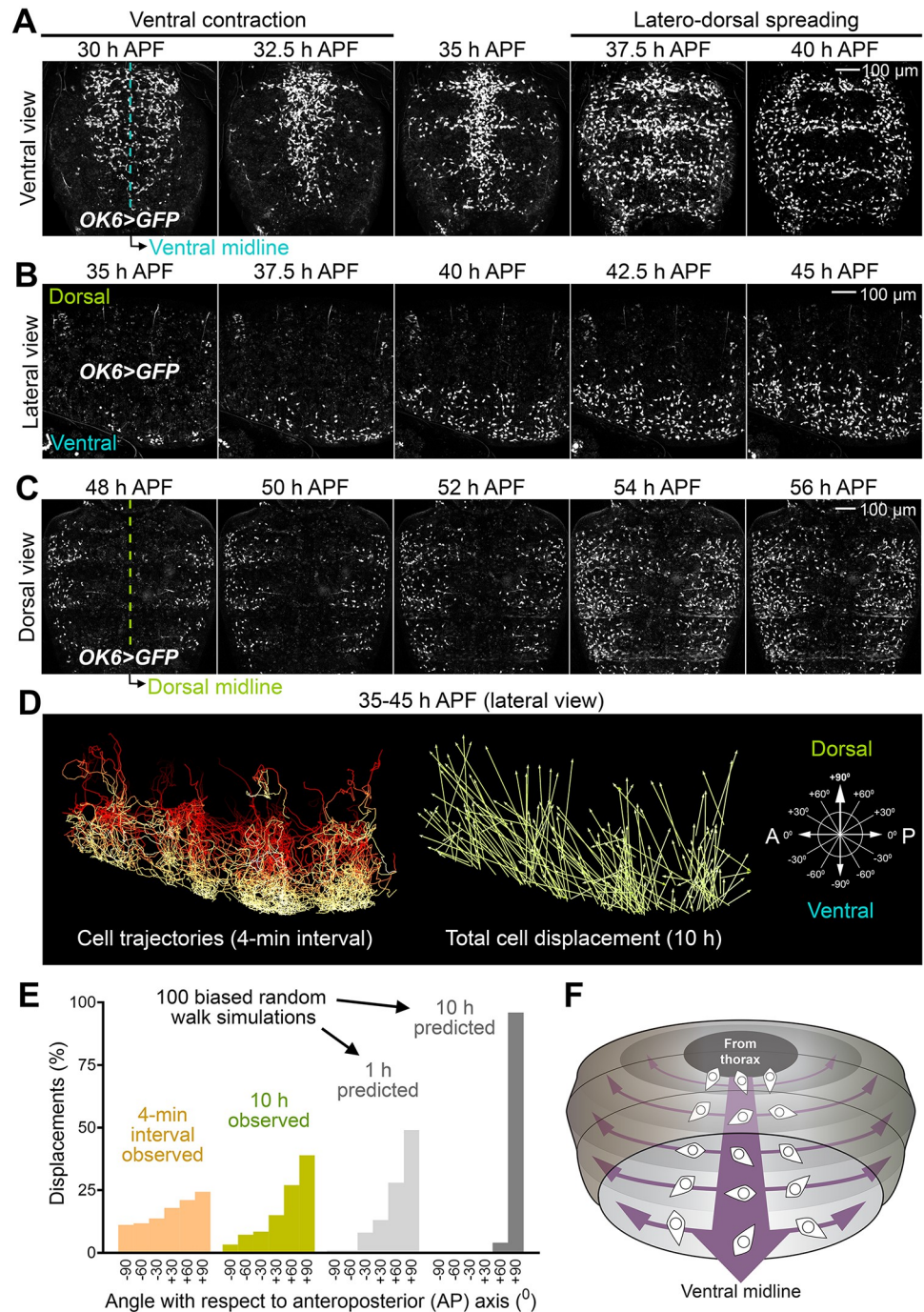


Fig 4. Adult fat body precursors spread from the ventral midline. (A) Still images from a time-lapse recording of adult fat body precursors (*OK6>GFP*, white) in the ventral abdomen of the pupa (30–40 h APF). Images are standard deviation projections of 62 confocal sections. See [S3 Video](#). (B) Still images from a time-lapse recording of adult fat body precursors (*OK6>GFP*, white) imaged laterally in the abdomen of the pupa (35–45 h APF; dorsal up, anterior left). Images are maximum intensity projections of 62 confocal sections. See [S3 Video](#). (C) Still images from a time-lapse recording of adult fat body precursors (*OK6>GFP*, white) in the dorsal abdomen of the pupa (48–56 h APF). Images are maximum intensity projections of 62 confocal sections. See [S3 Video](#). (D) Trajectories of the adult fat body precursors imaged in (B). On the left, complete migration paths are represented (a stack of images for each time point was acquired every 4 min). Total precursor displacement for the 10 h duration of recording is represented as well. See [S3 Video](#). (E) Graph representing the angle of migration of precursors in (B) with respect to the anterior-posterior axis. The angle of a fully dorsal displacement is 90° [see schematic representation in (D)]. For the 4-min interval angle distribution, $n = 22,831$. For the 10 h angle distribution, $n = 485$. Predicted distributions based on the assumption that migration is governed solely by dorsal displacement bias (no repulsion) are the result of 100 simulations in a biased

random walk model. In this model, cells migrate with constant speed and change direction every 4 min, with probabilities for the new migration angle given by the observed 4-min interval angle distribution (see [Materials and methods](#) and [S1 File](#)). (F) Schematic illustration of the migration of adult fat body precursors in the abdomen during metamorphosis. Precursors spread laterally and dorsally from the ventral midline. The data underlying the graphs in the figure can be found in [S1 Data](#).

<https://doi.org/10.1371/journal.pbio.3002050.g004>

a tendency towards displacements in the dorsal direction ([Fig 4E](#)). Consistent with both contact inhibition and guided migration governing precursor movement, the observed long-term displacement of precursors is less dorsally oriented than predicted by applying the observed 4-min directional bias in simulations of a biased random walk model ([Fig 4E](#); see [S1 File](#) and [Materials and methods](#) for details of the model). In all, our time-lapse recordings show that adult fat body precursors spread throughout the abdomen from the ventral midline ([Fig 4F](#)). In addition, our analysis of their trajectories indicates that a directional component guiding migration dorsally is operative besides mutual repulsion.

FGF signaling is required for adult adipogenesis

The spreading of adult fat body precursors from the ventral midline during metamorphosis, our live imaging showed, is very reminiscent of the migration of embryonic mesodermal cells during gastrulation, taking place after ventral furrow ingression [25]. Mesoderm migration in the embryo depends on FGF signaling. We therefore decided to test the involvement of FGF signaling in the adult fat body formation as well. Embryonic mesoderm cells express the FGF receptor Heartless (Htl) [26,27], whereas the overlying ectoderm expresses its FGF ligands Pyramus (Pyr) and Thisbe (Ths) [28,29]. Knock down of *htl* under control of *OK6-GAL4* in adult fat body precursors produced adults lacking most fat body tissue in their abdomens ([Fig 5A](#), [5B](#), and [5E](#)). Expression of a dominant negative version of Htl (Htl^{DN}) similarly caused a large reduction in adult fat body tissue ([Fig 5C and 5E](#)). Expression of a constitutively active Htl (Htl^{CA}), in contrast, did not cause any apparent defect ([Fig 5D and 5E](#)). Consistent with a requirement of *htl* in the formation of the adult fat body, an *htl-GAL4* reporter showed expression in the adult fat body precursors ([Fig 5F and S4 Video](#)). We next knocked down the expression of Htl-binding ligands Ths and Pyr ([Fig 5G](#)) under control of strong, ubiquitous driver *act-GAL4*. Knock down of *ths* strongly reduced the amount of fat body tissue in the adult abdomen ([Fig 5H and 5E](#); control in [S2A Fig](#)). Knock down of *pyr*, in contrast, did not show such effect ([Fig 5I](#)). Consistent with a requirement of *ths* in the formation of the adult fat body, a *ths-GAL4* reporter was expressed in the dorsal epidermis of the pupal abdomen ([Fig 5K and 5L](#)). Furthermore, adults where *ths* had been knocked down under control of dorsal epidermal driver *pnr-GAL4* presented a wide gap devoid of adult fat body around the dorsal midline ([Fig 5J and 5E](#); control in [S2A Fig](#)). Finally, overexpression of Ths in the wing epidermis under control of *rn-GAL4* caused the appearance of adult fat body between the dorsal and ventral surfaces of the wing ([Fig 5M and 5N](#)). Broadly complementary to *ths-GAL4*, a *pyr-GAL4* reporter showed expression in the ventral epidermis of the pupal abdomen ([S2B and S2C Fig](#)) despite a seeming lack of phenotype in *act>pyrⁱ* flies. In all, these data evidence that expression of FGF receptor Htl in adult fat body precursors and FGF ligand Ths in the epidermis are needed for correct formation of the adult fat body and suggest a role of Ths in directing the migration of adult adipocyte precursors.

FGF signaling confers directionality and substrate adherence during precursor spreading

We next tried to ascertain in more detail the role of FGF signaling in adult adipogenesis. To that end, we imaged and analyzed the migration of adult fat body precursors in conditions of

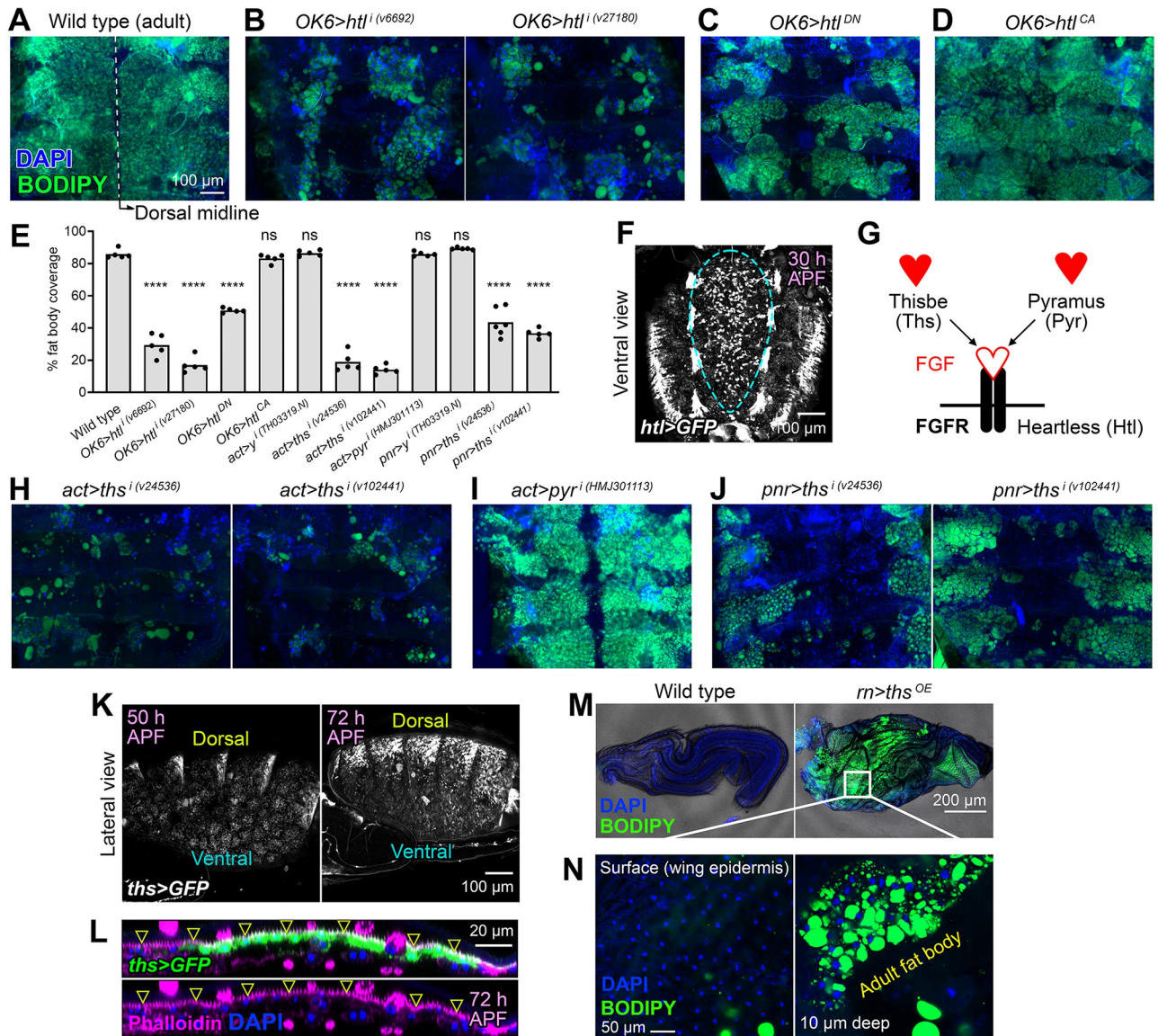


Fig 5. FGF signaling is required for adult adipogenesis. (A) Adult abdomen from a wild-type fly dissected 2 days after eclosion and mounted flat after staining with DAPI (nuclei, blue) and BODIPY (neutral lipids, green). (B) Adult abdomens from flies in which *htl* was knocked down under control of *OK6-GAL4* (*OK6>htlⁱ*) using 2 different RNAi transgenes. DAPI (blue) and BODIPY (green) stainings are shown. (C) Adult abdomen from a fly expressing dominant negative Htl (*OK6>htl^{DN}*). DAPI (blue) and BODIPY (green) stainings are shown. (D) Adult abdomen from a fly expressing a constitutively active Htl (*OK6>htl^{CA}*). DAPI (blue) and BODIPY (green) stainings are shown. (E) Quantification of adult fat body coverage measured in at least 5 individuals of the indicated genotypes, with the height of the bar indicating mean value. Significance of comparisons with the wild type in unpaired *t* tests reported as follows: n.s.: *p* > 0.05; ****: *p* < 0.0001. (F) Expression of GFP (white) under control of *htl-GAL4* in motile fat body precursors imaged in vivo 30 h APF in the abdomen (ventral view). Images are maximum intensity projections of 60 confocal sections. See S4 Video. (G) Cartoon representing the receptor Heartless (*htl*) and its 2 known FGF-like ligands Thisbe (*Ths*) and Pyramus (*Pyr*). (H) Adult abdomens from flies in which *ths* was knocked down under control of *act-GAL4* (*act>htlⁱ*) using 2 different RNAi transgenes. DAPI (blue) and BODIPY (green) stainings are shown. (I) Adult abdomen from a fly in which *pyr* was knocked down under control of *act-GAL4* (*act>pyrⁱ*). DAPI (blue) and BODIPY (green) stainings are shown. (J) Adult abdomens from flies in which *ths* was knocked down in the dorsal epidermis under control of *pnr-GAL4* (*pnr>thsⁱ*) using 2 different RNAi transgenes. DAPI (blue) and BODIPY (green) stainings are shown. (K) Expression of GFP (white) under control of *ths-GAL4* in the dorsal epidermis of the abdomen (lateral view) at 50 and 72 h APF. Images are maximum intensity projections of 60 confocal sections. (L) Z-section of an abdomen expressing GFP (green) under control of *ths-GAL4*, dissected 72 h APF and stained with F-actin dye phalloidin (magenta). GFP-positive cells are the outermost cells and display actin-rich apical trichomes (arrowheads). Nuclei stained with DAPI (blue). (M) Late pupal wings dissected from a wild-type pupa (left) and a pupa overexpressing *Ths* under control of *m-GAL4* in the wing blade (*m>ths^{OE}*, right), stained with BODIPY (green) and DAPI (blue). (N) Confocal sections of the region of the *m>ths^{OE}* wing indicated by the white square in (M), taken on surface (left, dorsal wing epidermis) and 10 μm depth (right, space between dorsal and ventral wing epidermal layers). BODIPY in green and DAPI in blue. Note that the small size of the fat body nuclei identifies these as adult adipocytes, not larval ones (see Fig 1D). The data underlying the graphs in the figure can be found in S1 Data.

<https://doi.org/10.1371/journal.pbio.3002050.g005>

loss of FGF signaling (expressing Htl^{DN} , Fig 6A) and excess FGF signaling (expressing Htl^{CA} , Fig 6B). In both cases, live imaging showed precursors spreading (Fig 6A–6C and S5 Video). Analysis of their direction of migration (4-min interval), however, revealed that expression of either Htl^{DN} or Htl^{CA} markedly reduced their tendency to displace dorsally (Fig 6D). This result is highly consistent with a role of dorsally expressed *Ths* in guiding the migration of *Htl*-expressing precursors as a chemoattractant cue. However, as previously noted, expression of Htl^{CA} in precursors produced a seemingly normal adult fat body (see Fig 5D), unlike Htl^{DN} (Fig 5C), hinting FGF roles additional or alternative to chemoattraction that might explain this discrepancy. To solve this, we further analyzed the spreading of $OK6>htl^{DN}$ and $OK6>htl^{CA}$ adult fat body precursors, and found that expression of Htl^{CA} , but not Htl^{DN} , reduced their migration speed (Fig 6E). Furthermore, counting of precursors in lateral view recordings from 48 to 58 h APF revealed that the number of precursors expressing Htl^{DN} decreased over time (Fig 6F), instead of increasing as a result of proliferation and income of new cells from the ventral side. Upon close observation, we discovered that precursors expressing Htl^{DN} frequently detached from the abdominal epidermis and abandoned the plane of view to disappear into the body cavity (Fig 6G and S6 Video). Altogether, our analysis of *htl* loss and gain of function phenotypes is consistent with a function of FGF signaling in both directing migration dorsally and increasing adhesion to the substrate.

Adult fat body adipocytes are formed by fusion of precursors after spreading

As a result of spreading and continued proliferation, adult fat body precursors end up covering most of the inner surface of the abdominal epidermis, stop migrating and become confluent at about 65 h APF, giving rise to a tissue monolayer (Fig 7A). Soon after becoming confluent, precursors start accumulating fat in the form of lipid droplets, suggesting a process of gradual differentiation into mature adipocytes, complete at day 2 after eclosion of the adult (Fig 7B). During this differentiation process, we noticed the progressive appearance of adipocytes containing 2 and 4 nuclei (Fig 7B), consistent with the observation of binucleate and tetranucleate adipocytes in the adult by others [30]. Indeed, our counts showed that the adult fat body consists entirely of binucleate and tetranucleate cells in proportions that do not seem to change after eclosion (Fig 7C). To ascertain the mechanism by which adult adipocytes become multinucleate, we imaged their late metamorphic development and documented multiple instances of cells merging through disappearance of the intervening plasma membranes (Fig 7D and S7 Video). These observations indicate that adult adipocytes become multinucleate not through mitosis followed by incomplete cytokinesis, as is the case in the mammalian liver [31], but as a result of cell fusion. In these binucleate and tetranucleate adipocytes, in addition, we found that the DNA content of nuclei in adults was 4C in average (Fig 7E). Furthermore, adult adipocyte nuclei were surrounded by a cortex of perinuclear microtubules (Fig 7F), typical of polyploid nuclei [32]. This suggests that adult adipocyte nuclei have switched to an endoreplicative cell cycle and, therefore, are tetraploid rather than diploid stalled in G2. Consistent with this, monitoring of the cell cycle with the FUCCI system [33] revealed that all nuclei in the mature adult fat body are found in G1 (S3 Fig). In summary, our data show that adult fat body precursors during late metamorphosis give rise through cell fusion to large binucleate and tetranucleate adipocytes whose nuclei are in turn tetraploid (Fig 7G).

The adult fat body buffers fat levels and provides resistance to starvation

After studying the morphogenesis of the adult fat body during metamorphosis, we sought to get insights into its function and evidence of its physiological importance. To this end, we

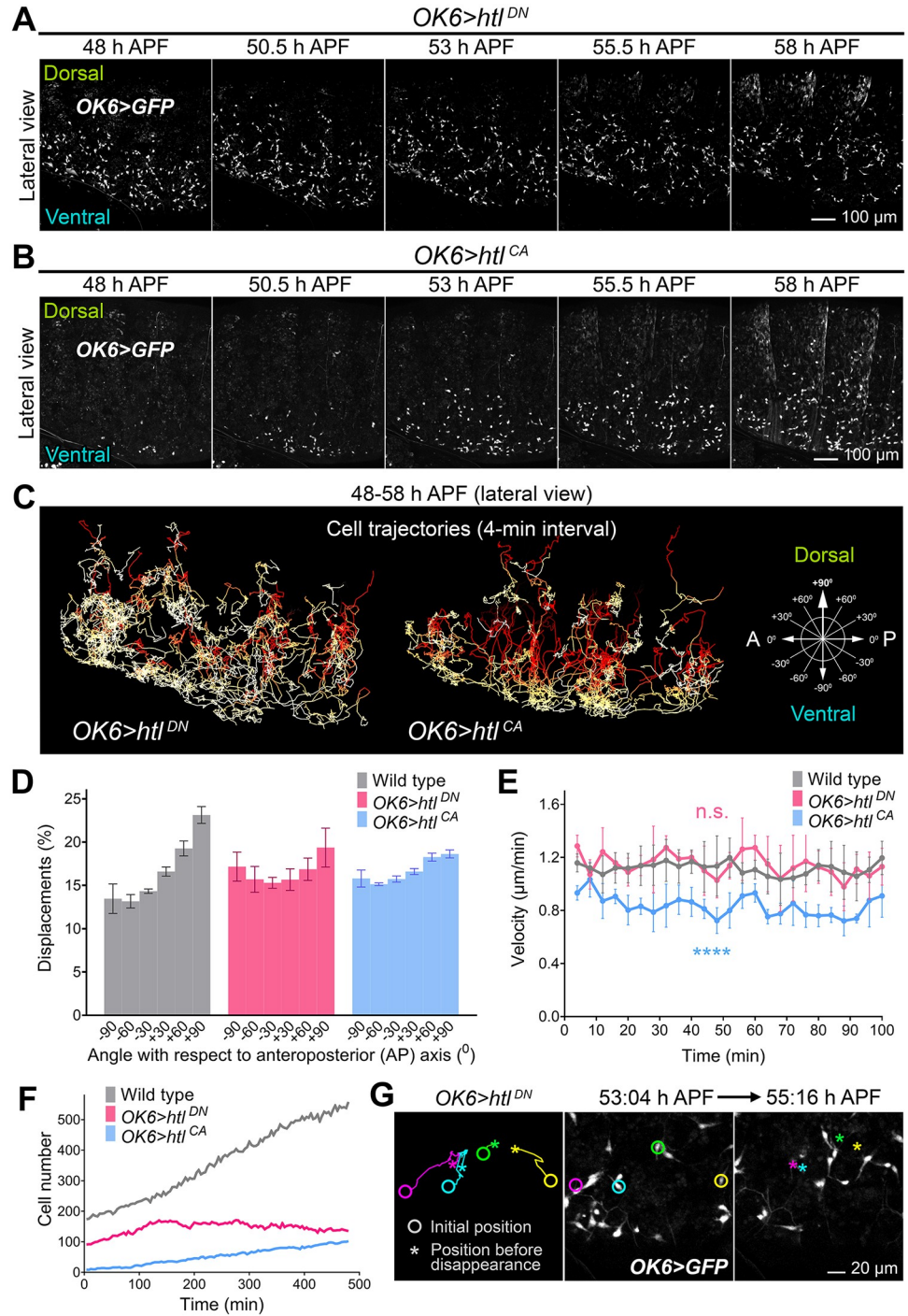


Fig 6. FGF signaling confers directionality and substrate adherence during precursor spreading. (A) Still images from a time-lapse recording of *OK6>htl^{DN}* adult fat body precursors (*OK6>GFP*, white) imaged laterally in the abdomen of the pupa (48–58 h APF; dorsal up, anterior left). Images are maximum intensity projections of 60 confocal sections. See [S5 Video](#). (B) Still images from a time-lapse recording of *OK6>htl^{CA}* adult fat body precursors (*OK6>GFP*, white) imaged laterally in the abdomen of the pupa (48–58 h APF; dorsal up, anterior left). Images are maximum intensity projections of 60 confocal sections. See [S5 Video](#). (C) Trajectories of the adult fat body precursors imaged in (A) and (B). Complete migration paths are represented (a stack of images for each time point was acquired every 4 min). See [S5 Video](#). (D) Angle of migration (4-min interval) with respect to the anterior-posterior axis of wild type, *OK6>htl^{DN}* and *OK6>htl^{CA}* precursors imaged laterally 52–54 h APF. Three recordings were analyzed for each genotype. Error bars represent SD. (E) Average migration velocity (4-min interval) of wild type, *OK6>htl^{DN}* and

OK6>htl^{CA} precursors imaged laterally 52–54 h APF. Three recordings were analyzed for each genotype. Error bars represent SD. Significance of differences with the wild type in two-way ANOVA tests reported in graph as follows: ****; $p < 0.0001$; n.s.: $p > 0.05$. (F) Evolution of precursor numbers with time in wild type, *OK6>htl^{DN}* and *OK6>htl^{CA}* abdomens imaged laterally 48–58 h APF. Notice stationary/decreasing number of *OK6>htl^{DN}* precursors. (G) Still images from a time-lapse recording of *OK6>htl^{DN}* adult fat body precursors (*OK6>GFP*, white) imaged laterally in the abdomen of the pupa (dorsal up, anterior left) at 53:04 (center panel) and 55:16 h APF. Initial position, trajectory, and final position before detachment of 4 precursors are represented in the left panel. Images are maximum intensity projections of 60 confocal sections. See [S6 Video](#). The data underlying the graphs in the figure can be found in [S1 Data](#).

<https://doi.org/10.1371/journal.pbio.3002050.g006>

analyzed adult flies in which the adult fat body was missing or severely reduced due to knock down of *srp* or *htl* under *OK6-GAL4* control. In these flies, we found that neutral lipids ectopically accumulated in oenocytes (Fig 8A), a cell type involved like the fat body in lipid metabolism [34]. This result suggests a central role for the adult fat body in storing away fat and buffering its circulation levels in the animal. Further proof of an essential storage role for the adult fat body, its fat content decreased when we subjected adults to starvation for 3 days and recovered normal levels when flies thus starved were refed for 1 day (Fig 8B and 8C). Reduction of fat levels upon starvation was accompanied by autophagy, as evidenced by the presence of vesicles positive for autophagy marker Atg8, reversible upon refeeding as well (Fig 8D and 8E). These results strongly argue that the adult fat body acts as an energy reserve to be mobilized upon starvation. To finally probe the importance of this reserve, we recorded the survival after starvation of wild-type flies and flies in which adult adipogenesis was impaired due to *srp* or *htl* knock down. We conducted these starvation experiments in the presence of *elav-GAL80*, inhibiting GAL4 expression in neurons, to avoid a possible influence of the expression of *OK6-GAL4* in motoneurons [22]. Compared to control flies, survival of flies in which *srp* or *htl* had been knocked under *OK6-GAL4* control was reduced (Fig 8F), showing that the adult fat body reserve provides increased resistance to starvation. In summary, we conclude that the adult fat body, formed de novo during metamorphosis, accomplishes a fat storage role crucial in the physiology of the adult.

Discussion

In this study, we found that adult *Drosophila* adipocytes do not originate in the larval adipose tissue. Instead, de novo adipogenesis takes place during metamorphosis, when the adult fat body assembles from undifferentiated mesodermal precursors. Through in vivo imaging, we observed that fast-proliferating adult fat body precursors migrate from the thorax into the abdomen, accumulate at the abdominal ventral midline and spread laterally and dorsally on the inner surface of the abdominal epidermis. The migration of these precursors is, therefore, strikingly reminiscent of mesoderm migration during gastrulation in the embryo [25,35,36]. During gastrulation, the cells that give rise to the mesoderm invaginate at the ventral midline, undergo epithelial-to-mesenchymal transition and migrate dorsally along the ectoderm. In light of the similarities between embryonic mesoderm migration and adult adipogenesis, we propose that the formation of the adult fat body in *Drosophila* is, in essence, a recapitulation of gastrulation that partially reenacts during metamorphosis that earlier process. Outside of insects, a form of secondary gastrulation has been reported during metamorphosis of the jellyfish *Aurelia* [37]. Another metamorphic process in *Drosophila* with a clear counterpart in embryonic development is thorax closure at the dorsal midline, reminiscent of embryonic dorsal closure and driven as well by JNK activity in an epidermal edge [38,39]. The extent to which metamorphosis recapitulates key morphogenetic processes of embryonic development is worth exploring. Indeed, comparisons among different *Drosophila* species revealed reduced

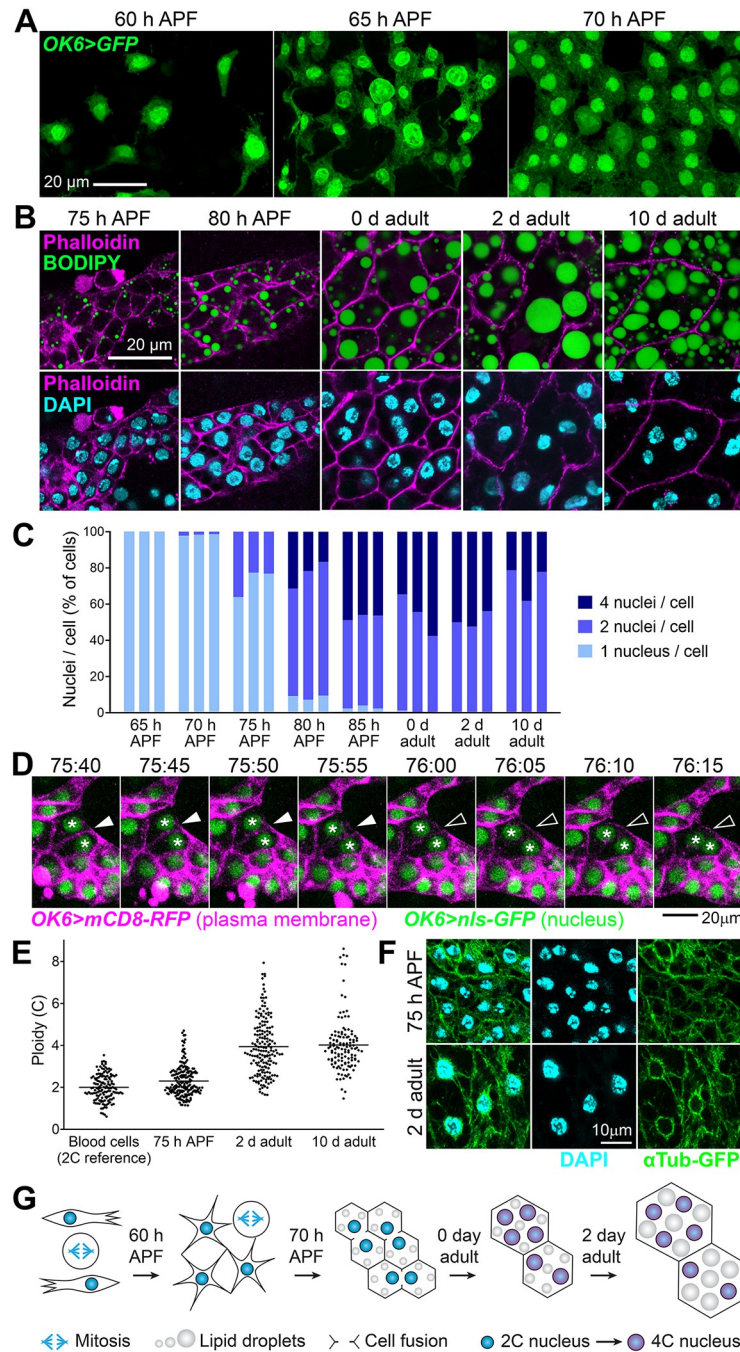


Fig 7. Adult fat body adipocytes are formed by fusion of precursors after spreading. (A) Adult fat body precursors (*OK6>GFP*, green) imaged at indicated times. Notice the presence of dividing cells. (B) Images showing the differentiation of adult precursors into mature adipocytes at indicated times. Eclusion of the adult takes place at about 96 h APF. Stainings with phalloidin (actin cell cortex, magenta, upper and lower row), BODIPY (neutral lipids, green, upper row) and DAPI (nuclei, cyan, lower row) are shown. Notice gradual fat accumulation, cell size increase and appearance of binucleate and tetranucleate cells until day 2 of eclosion. (C) Proportion of cells containing 1, 2, and 4 nuclei at indicated times. Counts in 3 individuals per time point are represented. At least 100 cells were analyzed per individual at 70 and 75 h APF, 40 cells at 80 and 85 h APF, and 30 cells in adults. (D) Still images from a time-lapse recording of the fusion of 2 adult fat body precursors at indicated times (75:40–76:15 h APF). Plasma membrane is labeled with *mCD8-RFP* (magenta) and nuclei with *nls-GFP* (green), both driven by *OK6-GAL4*. Arrowheads point to the disappearing membrane separating the 2 cells. Asterisks mark their nuclei. See [S6 Video](#). (E) Ploidy in nuclei of adult adipocytes at indicated times. Ploidy was estimated from confocal stacks by measuring the amount of DAPI signal through the entire nuclear volume (see [Methods](#)). Blood cells were used as a diploid reference (2n, 2C). Each

point represents a measurement in a single nucleus. Horizontal lines mark the average value. (F) Microtubule organization in adult adipocytes at 75 h APF (upper row) and 2 days after eclosion (lower row). Microtubules are marked with α Tub-GFP (green) driven by *OK6-GAL4* and *Cg-GAL4*, respectively. Nuclei stained with DAPI (cyan). Notice perinuclear microtubule organization in 2 day adult nuclei. (G) Cartoon depicting the maturation of adult fat body precursors into adipocytes. Migrating adult fat body precursors migrate and divide until reaching confluence, when they start accumulating lipid droplets and fusing, giving rise to binucleate and tetranucleate adipocytes. During or after the cell fusion period, nuclei undergo 1 additional round of DNA replication and become tetraploid. The data underlying the graphs in the figure can be found in [S1 Data](#).

<https://doi.org/10.1371/journal.pbio.3002050.g007>

transcriptome divergence during both mid-embryogenesis [40] and metamorphosis [41], suggesting intense developmental constraints shared by both stages.

Supporting the notion that adult adipogenesis recapitulates embryonic mesoderm formation, we found that FGF signaling, required for mesoderm migration, is critical also for adult fat body formation. In both processes, epidermal FGF ligands seem to activate FGF receptor Htl in motile precursors. In the embryo, FGF signaling mutants fail to spread their mesoderm from the ventral midline. Different roles have been attributed to FGF to explain this defect, such as promoting epithelial-to-mesenchymal transition, regulating proliferation and guiding migration as a chemoattractant cue [35,42]. According to our results, FGF may not affect precursor proliferation or differentiation during adult adipogenesis. However, our findings show that FGF acts as a chemoattractant cue that influences the direction of migration, since both loss and gain of *htl* function makes precursor displacements less dorsally directed. In agreement with such a guidance role, a GAL4 expression reporter for FGF *Ths* is expressed in the dorsal epidermis and knock down under control of dorsal epidermal driver *pnr-GAL4* produced fat body reduction. It would be convenient, however, to confirm this expression pattern through other means. Similarly, our assessment of *htl* and *pyr* expression, in adult adipocyte precursors and ventral epidermis, respectively, is based as well on GAL4 reporters.

Our analysis reveals that a second effect of FGF signaling, potentially more important for adult adipogenesis, is to enhance adhesion between precursors and the epidermis on which they migrate. This conclusion is based on (1) the behavior of *htl^{DN}* precursors, which frequently detach and disappear into the body cavity; (2) the decreased migration speed of *htl^{CA}* precursors; and (3) the fact that *htl^{CA}* precursors give rise to an apparently normal adult fat body despite decreased motility and directionality. In this light, mutual repulsion and contact inhibition of locomotion, similar to the dispersion of embryonic blood cells [43], may be sufficient to ensure spreading of *htl^{CA}* precursors, although at a slower pace. In embryonic mesoderm spreading, one of the defects reported in *htl* mutants is reduced expression of *mys*, encoding a β subunit of the extracellular matrix receptor integrin [44]. Reduced integrin adhesion could explain the detachment of *Htl^{DN}* precursors, but does not fit well their normal velocity, as loss of integrin should reduce migration speed. A recently described process in which FGF may predominantly regulate adhesion instead of acting as a guidance cue is the wrapping of olfactory glomeruli expressing *Ths* by *Htl*-expressing ensheathing glia [45]. In these and other processes, the mechanisms by which FGF signaling regulates substrate adherence are unclear. To address this, migration of adult adipocyte precursors, suitable for long-term live imaging of large numbers of migrating cells and complex genetic manipulations, could be a useful system to elucidate the effects of FGF signaling on migration and the specificity of the roles of ligands *Ths* and *Pyr*, still not well understood in the embryo. In this regard, the complementary expression in the pupal abdomen of *ths-GAL4* (dorsal) and *pyr-GAL4* (ventral) is reminiscent of the situation in the embryonic epidermis, where both *Ths* and *Pyr*, complementarily expressed as well, are required for correct mesoderm migration, which warrants further examination of the role of *pyr* in adipocyte migration despite a seeming lack of effect in *act>pyr^f* flies.

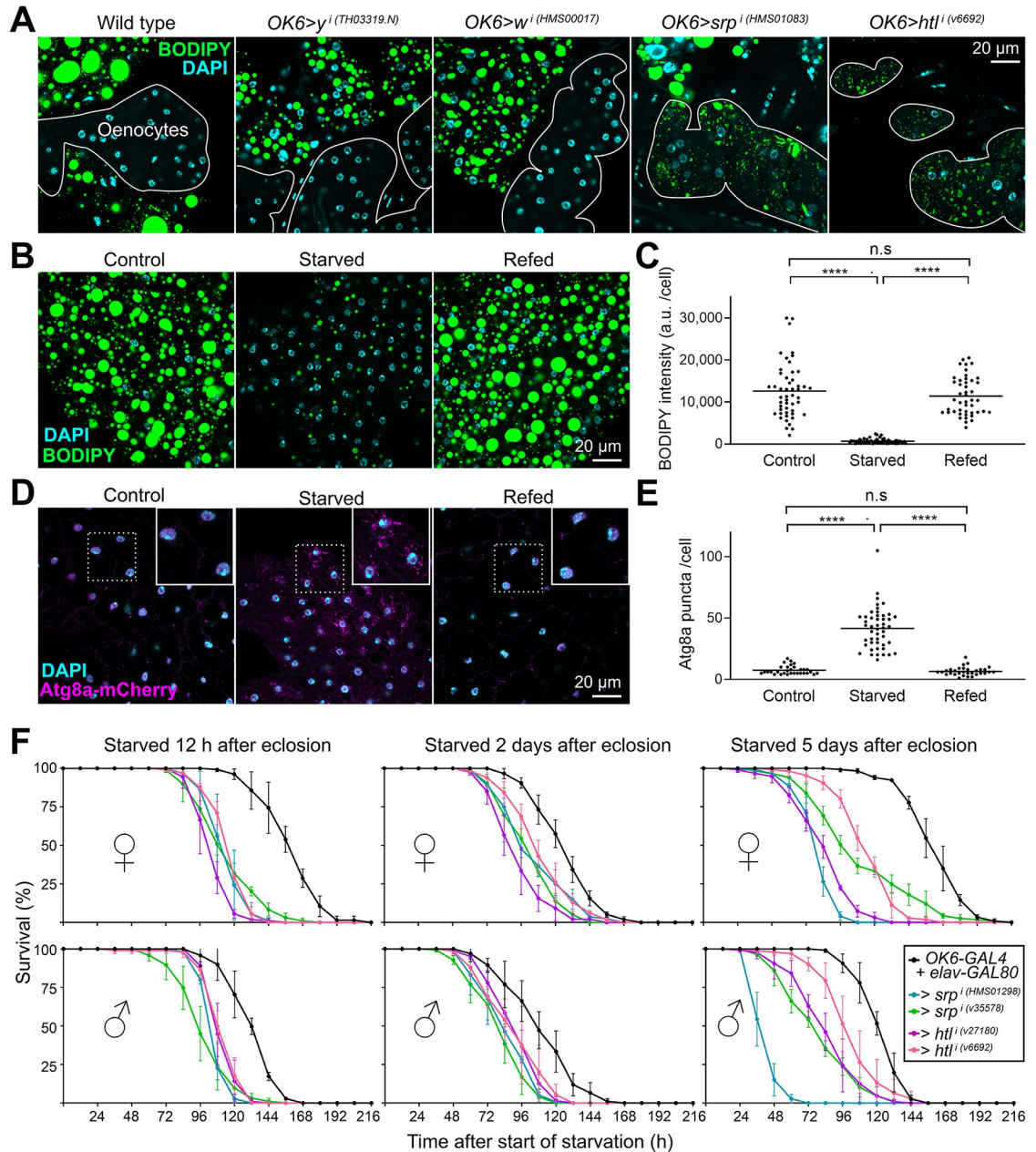


Fig 8. The adult fat body buffers fat levels and provides resistance to starvation. (A) Oenocytes (outlined) from adult wild type, *OK6>yⁱ* and *OK6>wⁱ* control, *OK6>srpⁱ* and *OK6>htlⁱ* abdomens dissected 2 days after eclosion, stained with BODIPY (green) and DAPI (cyan). Notice the accumulation of lipid droplets in *OK6>srpⁱ* and *OK6>htlⁱ* oenocytes. (B) Adult fat body stained with BODIPY (green) in control flies (5-day adult, left panel), starved flies (2-day adult starved for 3 days, center panel) and refed flies (2-day adult starved for 3 days and refed for 1 day, right panel). Nuclei stained with DAPI (cyan). (C) Quantification of BODIPY staining in the experiment in (B). Each dot represents BODIPY signal intensity measured in 1 cell, with the horizontal bar indicating mean value. Significance of comparisons in Mann-Whitney tests as follows: n.s.: $p > 0.05$; ****: $p < 0.0001$. (D) Adult fat body expressing autophagy marker Atg8a-mCherry (driven by *BM-40-SPARC-GAL4*, magenta) in control flies (5-day adult, left panel), starved flies (2-day adult starved for 3 days, center panel) and refed flies (2-day adult starved for 3 days and refed for 1 day, right panel). Areas inside dashed squares are magnified in upper right corner insets. Nuclei stained with DAPI (cyan). (E) Quantification of autophagy induction in the experiment in (D). Each dot represents number of Atg8a-mCherry-positive puncta counted in 1 cell, with the horizontal bar indicating mean value. Significance of comparisons in Mann-Whitney tests reported as follows: n.s.: $p > 0.05$; ****: $p < 0.0001$. (F) Graphs representing survival of control, *OK6>srpⁱ* and *OK6>htlⁱ* adult male (upper graphs) and female (lower graphs) flies subjected to starvation starting 12 h (left), 2 days (center), and 5 days (right) after eclosion. *elav-GAL4*, repressing GAL4 activity in neurons, was included in genotypes to prevent a possible influence of *OK6-GAL4* expression in larval motoneurons [22]. Three repeats were carried out per genotype and sex, each with at least 85 flies. Error bars represent SD. In all

cases, differences with the control were significant in Mantel–Cox tests (****; $p < 0.0001$). The data underlying the graphs in the figure can be found in [S1 Data](#).

<https://doi.org/10.1371/journal.pbio.3002050.g008>

Another point for future clarification is the exact origin of adult fat body precursors and their location prior to migration into the abdomen. This, however, will require additional markers and better knowledge of adult fat body specification. *OK6-GAL4*, an insertion into the promoter of the gene *RapGAP1* [22], allowed us to follow the development of adult fat body precursors into adult adipocytes during metamorphosis. However, *OK6-GAL4* expression in these cells does not start until around 12 h APF. Furthermore, a previous study reported that null mutants for *RapGAP1*, encoding a GTPase activating protein for small GTPase Rap1, were viable and showed no detectable phenotypic abnormalities [46], suggesting that this gene may not have a role in the specification of these cells as adipocyte precursors. Our experiments do not support a role for *Srp* in adult adipocyte specification either, since null mutant *srp* precursors seem to be capable of correctly differentiating. Our results, however, evidence reduced rates of cell division in precursors upon *srp* knock down, indicating a role of *Srp* in the proliferation of these cells, and probably also in their survival, as suggested by the occasional observation of apoptotic precursors in this condition. It would be interesting to test, in addition, whether *Srp* is required to establish or maintain *htl* expression, given that precursor migration is visibly impaired in live recordings of *OK6>srpⁱ* animals.

Lineage tracing experiments with *Mef2-GAL4* suggest a common lineage with the myoblast precursors of adult muscles. It has been proposed that adult fat body cells derive from ad epithelial cells [18]. These are populations of cells in the larval imaginal discs that contain large numbers of adult muscle precursors. According to the images in the reference, however, the putative precursor cells are not ad epithelial cells, but differentiated blood cells that typically attach to other regions of the imaginal discs such as the wing pleura or the antenna. Despite this, we consider imaginal disc-associated ad epithelial cells a possible source of adult adipocyte precursors. Similar to the adipogenic precursors, ad epithelial myoblasts express *Htl* and respond to the expression of FGF ligands in the epidermis [47–49]. Further suggesting similarity between fat body and muscle precursors is production of syncytia through cell fusion. Adipocyte fusion, however, seems homotypical, unlike myoblast fusion, in which a founder asymmetrically instructs other cells to fuse with it [50]. It will be interesting to investigate in the future how the temporal window of adipocyte cell fusion is determined (70 to 96 h APF) and whether the conserved machinery by which myoblasts fuse to produce muscle fibers is acting in adipocyte fusion as well.

The consequences and potential advantages for the function of adipocytes of their status as binucleate and tetranucleate polyploid cells is an additional topic of interest stemming from our findings. Human and rodent hepatocytes are frequently binucleate, but this is due to abortive cytokinesis rather than cell fusion [31]. Moreover, in the human liver endoreplication produces tetraploid and octaploid nuclei, giving rise to a mixture of mononucleate 2n, 4n, 8n and binucleate 2x2n, 2x4n cells [51]. Faster attainment of large cell volumes is often adduced to explain polyploidy in the larval fat body and other endoreplicating larval tissues [52], a purpose cell fusion could serve as well. Alternatively, it has been proposed that polyploidy confers protection to human hepatocytes against genotoxic damage. Under this lens, acquiring multiple genome copies could buffer the effects of mutations caused by DNA damaging agents [53]. Regardless of the reasons behind multinucleation/polyploidy in the adult fat body, a possible consequence, our results suggest, is limited tissue plasticity. We did not observe after eclosion mitotic cells, nor any variation in nuclei number, DNA content (4C) or proportions of binucleate/tetranucleate cells. Starvation did not seem to induce changes in these features either.

Starvation and refeeding, however, did decrease and increase cell size, respectively. It is likely, therefore, that adult fat body remodeling can take place only through changes in cell size, not in cell or nuclear number. However, further experiments should test the possibility that stimuli such as excess nutrition, damage, or traumatic tissue loss might induce remodeling or regrowth through endoreplication, polyploid mitosis, depolyploidizing divisions, or reactivation of cell fusion. Additionally, in light of the possibly low plasticity of the adult fat body, an interesting question to ask is whether the diet of the larva could imprint the metabolic status of the adult by affecting adult fat body development, for instance, by influencing the initial number of precursors or their proliferative potential.

Despite our data showing that adult adipocytes do not derive from larval adipocytes, functional relations between these 2 separate adipocyte populations during the time they coexist is an interesting topic deserving of further investigation. We observed that adult adipocytes increase their size from 0 to 2 days after eclosion, consistent with previous reports [54] and coincident with the final disappearance of the dissociated larval adipocytes, suggesting a transfer of their fat content to the adult fat body. Indeed, a role in resistance of the adult to starvation has been postulated for these larval adipocytes persisting in the body cavity in the eclosed adult [55]. This is based on experiments where survival of starved flies was reduced in older adults with respect to younger ones starved since eclosion. Our own starvation experiments, however, did not find such effect, as flies starved since day 5 after eclosion were no less resistant than those starved from day 2 or day 1. Alternatively, dissection of the influence of the larval fat body on adult fat body development or adult physiology could come from experiments in which the elimination of larval adipocytes is prevented. We were, however, unsuccessful in delaying the disappearance of the larval fat body beyond day 2 through expression of p35 or DIAP1, inconsistent as well with a previous report [55].

Besides characterizing adult fat body development, we importantly provide evidence of its physiological significance, for which conclusive prove had remained elusive. We found that flies where the adult fat body was missing or reduced (upon *srp* or *htl* knock down) displayed accumulation of neutral lipids in oenocytes and decreased viability upon starvation, demonstrating an essential role of the adult fat body as a lipid store and energy reserve. Consistent with this, starvation induced adult adipocyte autophagy and reduction in fat content, both reversible upon refeeding. By generating flies specifically lacking adult fat body, finally, our study opens new avenues to systematically research adipocyte function in the adult, including roles beyond storage and metabolic regulation, for instance, in endocrine signaling, matrix production, detoxification, immune responses, reproduction, and mating and feeding behaviors.

Methods

Drosophila genetics

Standard fly husbandry and genetic methodologies were used to obtain the required genotypes for each experiment (see [S1 Table](#) for a detailed list of experimental genotypes). Fly strains and genetic crosses were maintained on standard medium prepared in our laboratory with yeast (24.5 g/L), cornmeal (50 g/L), agar (10 g/L), white granulated sugar (7.25 g/L), brown granulated sugar (30 g/L), propionic acid (4 mL/L), methyl-4-hydroxybenzoate (1.75 g/L), and absolute alcohol (17.5 mL/L). Pupae were staged by collection at the white pupa stage (0 h APF). Adults were staged by collection of newly eclosed animals from vials emptied at least 4 h before (day 0 adult). Only males were imaged and analyzed, except for the survival experiment in [Fig 8F](#), in which both males and females were separately subjected to starvation. The GAL4-UAS system was employed to drive UAS transgene expression under the control of GAL4 drivers. Crosses were maintained at 25 °C except for lineage tracing experiments involving *tub-*

GAL80^{ts}, in which cultures were maintained at 18 °C until transferred to 30 °C to initiate GAL4-driven gene expression. In lineage tracing experiments, expression of the yeast recombinase Flp driven by *twi-GAL4* or *Mef2-GAL4* excises an FRT-flanked sequence in a GAL4 flip-out cassette [56], turning on permanent, inheritable GAL4 expression in the affected cells and their progeny even after *twi-GAL4* or *Mef-GAL4* have ceased to be expressed in them. The time of labeling was additionally controlled with thermosensitive GAL4 repressor *tub-GAL80^{ts}* by staging and transferring animals from 18 °C to 30 °C at L1, L2, L3, or white pupa stage (0 h APF). Negatively labeled mitotic recombination clones (Figs 3 and S1G) were generated through the Flp/FRT system [57]. The following strains were used:

w; *OK6-GAL4* (BDSC, 64199),
w; *UAS-GFP.S65T* (BDSC, 1521),
w; *UAS-myr-RFP / TM6B* (BDSC, 7119),
w; *Cg-GAL4* (BDSC, 7011),
ppl-GAL4 (Gift from Pierre Leopold),
w twi-GAL4 (BDSC, 914),
y w; *ay-GAL4 UAS-GFP.S65T / CyO* (BDSC, 4411),
w; *Sco / CyO; tub-GAL80^{ts}* (BDSC, 7018),
y w; *Mef2-GAL4* (BDSC, 27390),
w¹¹¹⁸ (BDSC, 3506),
y v sc sev; *UAS-w.RNAi^{TRiP.HMS00017}* (THFC, THU0558),
y v sc sev; *UAS-y.RNAi^{TH03319.N}* (THFC, TH03319.N),
y v sc sev; *UAS-srp.RNAi^{TRiP.HMS01298}* (THFC, THU1529),
y v sc sev; *UAS-srp.RNAi^{TRiP.HMS01083}* (BDSC, 34080),
w; *UAS-srp.RNAi^{VDRC.v35578}* (VDRC, v35578),
w; *FRT82B Ubi-GFP* (BDSC, 5188),
y w; *FRT82B* (gift from Tian Xu),
y w; *UAS-Flp / CyO* (BDSC, 4539),
srp⁰¹⁵⁴⁹ / TM3, Sb (BDSC, 11538),
w; *UAS-htl.RNAi^{VDRC.v6692}* (VDRC, v6692),
w; *UAS-htl.RNAi^{VDRC.v27180}* (VDRC, v27180),
y w; *UAS-htl.DN.M; UAS-htl.DN.M* (BDSC, 5366),
w; *UAS-htl.lambda.M* (BDSC, 5367),
w; *GMR93H07-GAL4* (BDSC, 40669),
y w; *act5C-GAL4 / TM6B* (BDSC, 3954),
w; *UAS-ths.RNAi^{VDRC.v24536} / TM3* (VDRC, v24536),
y w; *UAS-ths.RNAi^{VDRC.v102441}* (VDRC, v102441),

y w; *UAS-pyr.RNAi^{TRiP.HMJ30113}* / *CyO* (BDSC, 63547),
y w; *pnr-GAL4* / *TM3,Ser* (BDSC, 3039),
w; *ths^{MI07139-TG4.1}* / *CyO*; *MKRS* / *TM6B* (BDSC, 77475),
w; *rn-GAL4* / *TM3,Sb* (BDSC, 7405),
w; *UAS-ths.S* (BDSC, 93874),
y w; *UAS-mCD8-GFP* (BDSC, 5137),
w; *UAS-GFP.nls* (BDSC, 4776),
w; *UAS-mCD8-RFP* (BDSC, 32219),
w; *UAS-GFPS65C.αTub84B* / *CyO* (BDSC, 7374),
BM-40-SPARC-GAL4 (gift from Hugo Bellen),
y w; *UAS-mCherry.Atg8a* (BDSC, 37750),
w; *elav-GAL80* (gift from Bing Zhou),
w; *UAS-GFP.E2F1.1–230* *UAS-NLS.CycB.1-266* / *CyO*; *MKRS* / *TM6B* (BDSC, 55110),
y w; *pyr^{CR01744-TG4.2}* / *SM6a* (BDSC, 91292).

Tissue dissections

To dissect pupal abdomens, we attached pupae to glass slides through their ventral sides using double-sided sticky tape. Then, we proceeded to open and peel the pupal case with fine tip forceps, pull out the animal carefully, and transfer it to a Sylgard plate filled with PBS for dissection. Using dissection scissors, we separated the abdomen from the thorax and cut open the abdomen on its ventral side. Afterwards, we removed guts, gonads, larval fat body, and other inner tissues using forceps. Abdomens were then fixed in 4% PFA for 15 min and washed twice in PBS for 15 min. After this, abdomens were either further processed for tissue staining (see below) or mounted flat for direct observation with their inside surface up on a glass slide in a drop of DAPI-Vectashield (Vector Laboratories). A similar strategy was used for dissecting adult abdomens, only flies were immobilized by anesthetization with CO₂, not stuck to a glass slide with tape.

Tissue stainings

For neutral lipid stainings, fixed pupal and adult abdomens were stained in BODIPY 493/503 (1:3,000 dilution of a 1 mg/mL stock, Life Technologies) in PBS for 1 h at room temperature and washed twice in PBS for 10 min before mounting in DAPI-Vectashield. For double staining of neutral lipids and actin cortex (Fig 7B), we stained fixed pupal and adult abdomens with Texas-Red phalloidin (1:100, Life Technologies) and BODIPY 493/503 (1:3,000 dilution of a 1 mg/mL stock, Life Technologies) in PBT (PBS containing 0.1% Triton X) for 2 h at room temperature, followed by PBS washes (3 × 20 min). For single phalloidin stainings (Figs 5L and S2C), we stained fixed pupal abdomens with Texas-Red phalloidin (1:100, Life Technologies) in PBT for 2 h at room temperature, followed by PBS washes (3 × 20 min). For anti-Srp antibody staining (Figs 2A and S1A), fixed samples were blocked in PBT-BSA (PBS containing 0.2% Triton X-100 detergent, 1% BSA, and 250 mM NaCl) for 1 h, incubated overnight with anti-Srp primary antibody (1:200) in PBT-BSA at 4 °C, washed in PBT-BSA (3 × 20 min),

incubated for 2 h in anti-rabbit IgG conjugated to Alexa-555 (1:200, Life Technologies) in PBT-BSA at room temperature, and washed in PBS (3×10 min). For staining of apoptotic adult fat body precursors (S1C Fig), fixed pupal abdomens were permeabilized overnight in PBT-BSA at 4 °C, incubated in TUNEL mixture (One Step TUNEL Apoptosis Assay Kit, red fluorescence, Beyotime Biotechnology) for 1 h at 37 °C and washed in PBT-BSA (3×10 min). All samples were finally mounted in DAPI-Vectashield.

Imaging of fixed tissues and analysis

Images of fixed adult abdomens stained with BODIPY in Figs 2B, 5A–5D, 5H–5J, S1E, and S2B were acquired in a Zeiss Axio Imager D.2 epifluorescence microscope using a $10 \times / NA$ 0.3 objective. Other images of fixed pupal and adult abdomens were acquired with a Zeiss LSM780 confocal microscope using $10 \times / NA$ 0.3, $20 \times / NA$ 0.8, $40 \times / NA$ 1.2 (water), or $63 \times / NA$ 1.4 (oil) objectives. Nuclear counts in Fig 7C were performed using the Multi-point tool in ImageJ-FIJI software. These counts were conducted on confocal stacks of images showing nuclear DAPI signal and plasma membrane *OK6>mCD8-GFP* (pupae) or phalloidin (adults). Three individuals were analyzed for each developmental time point. For nuclear ploidy estimation in Fig 7E, confocal stacks of DAPI images were outlined and labeled with the Surface function in Imaris 9.8.1 software (Bitplane) and total DAPI signal inside the nucleus was computed. Ploidy was calculated with reference to the average DAPI fluorescence value of diploid (2n, 2C) blood cells. For quantification of BODIPY in Fig 8C, signal intensity was measured in individual cells using ImageJ-FIJI in 3 images per condition. For quantification of autophagy in Fig 8E, the number of cytoplasmic Atg8a-mCherry puncta in cells was manually counted using the Multi-point tool of ImageJ-FIJI in 3 images per condition.

Live imaging and analysis

For live imaging of adult fat body formation during metamorphosis, pupae were removed completely from the pupal case with forceps and deposited on a glass-bottomed dish with a small drop of halocarbon oil 700 (Sigma) placed between the glass and the area to image. At the time of imaging, the glass-bottomed plate was inverted, leaving the animal hanging from the glass, attached to it by the surface tension of the oil. To maintain humidity, a piece of paper tissue soaked with water was located inside the dish. Imaging was conducted at a room temperature of 23 °C in a Zeiss LSM780 confocal microscope using a $10 \times / NA$ 0.3 objective for recordings of precursor migration (S1–S6 Videos), counting of *OK6>srpⁱ* precursors (Fig 2D) and documentation of *htl*, *ths*, and *pyr* expression (Figs 5F, 5K, and S2B). For quantification of adult fat body reduction (Figs 2C, 5E, and S1F), we measured the area covered by fat body in images like those in Figs 2B, 5A–5D, 5H–5J, and S1E in at least 5 individuals per genotype. Number of precursors at 30 h APF and 36 h APF in wild type and *OK6>srpⁱ* animals were counted using the Multi-point tool in ImageJ-FIJI software. A $40 \times / NA$ 0.95 (air) objective was used for recordings of precursor fusion (S7 Video). From confocal stacks, maximum intensity projections or standard deviation projections were obtained using Zeiss Zen software. In recordings of precursor migration, 60 to 65 confocal sections were acquired per time point with a z-step of 1.7 to 2.0 μm at intervals of 4 min. In ventral view recordings and imaging in vivo (Figs 1E, 2D, 4A, and 5F), the legs were carefully displaced anteriorly, out of the imaging frame. For recordings of precursor fusion, 16 confocal sections were acquired per time point with a z-step of 1.2 μm at intervals of 5 min.

Videos of maximum intensity or standard deviation projections were imported into Imaris 9.8 software to analyze precursor migration. The Spots tool was used to track cells and generate trajectories with the following parameters: 20 μm maximum distance between successive time

points, 2 time points maximum gap size, and 10 time points minimum track duration. Raw data for cell position was exported from Imaris into Excel, where we obtained displacement angles and speed through basic trigonometric calculations.

Biased random walk simulation

To simulate paths of cell migration and predict 1-h and 10-h distribution of displacement angles in Fig 4E, we devised a simple biased random walk model, implemented through an Excel formula contained in S1 File. In this model, cells migrate with a constant speed of 1 au/4 min and change their migration angle every 4 min, with the probabilities of the new angle given by the 4-min distribution of displacement angles observed in live recordings (also in Fig 4E). Plotted predicted distributions correspond to 100 simulations.

Starvation assays

Starvation/refeeding experiments in Fig 8B and 8D were conducted by placing 12-h, 2-day and 5-day-old male adults on starvation medium (2% agar medium) for 3 days before dissection. For refeeding, animals starved as above were transferred back to standard medium and then dissected. For survival tests in Fig 8F, 2-day adults were placed on starvation medium and the number of surviving flies were counted at 12 h intervals. Three replicates of the experiment were performed separately for males and females, each replicate consisting of 2 vials containing 15 to 20 animals. Significance of differences with the control was tested through Mantel-Cox tests using GraphPad Prism 8. All differences were significant (***; $p < 0.0001$).

The numerical data used in all figures are included in S1 Data.

Supporting information

S1 Fig. Srp is required for amplification of adult fat body precursors (related to Figs 2 and 3). (A) Adult fat body precursors (*OK6-GAL4*-driven GFP, green) in wild-type control (left) and *OK6>srpⁱ* (right) abdomens dissected 72 h APF and stained with anti-Srp antibody (magenta). (B) Still images from movies recorded between 30 and 36 h APF showing examples of cell division in adult fat body precursors (*OK6-GAL4*-driven GFP, white) from wild-type control and *OK6>srpⁱ* animals. See also S2 Video. (C) TUNEL apoptosis staining (magenta) of adult fat body precursors (*OK6-GAL4*-driven GFP, green) from wild type, *OK6>srpⁱ* and *OK6>htlⁱ* abdomens dissected 36 h APF. Apoptotic precursors (arrowheads) were observed in 3 out of 10 *OK6>srpⁱ*. (D) Quantification of TUNEL-positive apoptotic adult fat body precursors in abdomens dissected 36 h APF of the indicated genotypes. Each dot represents the percentage of TUNEL positive precursors in 1 individual. Between 40 and 241 precursors were scored per individual. (E) Adult abdomens from control, *OK6>srpⁱ* and *OK6>htlⁱ* flies, all expressing apoptosis inhibitor p35 under *OK6-GAL4* control. Tissues stained with DAPI (nuclei, blue) and BODIPY (neutral lipids, green). (F) Coverage of adult fat body measured in images like those in (E) in at least 5 individuals per genotype, with the height of the bar indicating mean value. p35 expression shows no significant effect on *OK6>srpⁱ* and *OK6>htlⁱ* phenotypes (unpaired *t* tests; n.s.: $p > 0.05$). Data for *OK6>srpⁱ* and *OK6>htlⁱ* from Figs 2C and 5E, respectively. (G) High magnification view of *srp⁰¹⁵⁴⁹* homozygous adult adipocytes generated in wild-type animals through mitotic recombination (see Fig 3). Mutant cells are negatively labeled by loss of Ub-GFP (green). *OK6-GAL4*-driven myr-RFP in magenta. Nuclei stained with DAPI (white). Asterisks mark circular spaces in the cytoplasm indicative of lipid droplets. The data underlying the graphs in the figure can be found in S1 Data.

(TIF)

S2 Fig. RNAi controls and *pyr-GAL4* expression (related to Fig 5). (A) Adult abdomens from control flies in which *yellow* was knocked down under control of *act-GAL4* (*act>yⁱ*) and *pnr-GAL4* (*pnr>yⁱ*). DAPI (blue) and BODIPY (green) stainings are shown. (B) Expression of GFP (white) under control of *pyr-GAL4* in the ventral epidermis of the abdomen (lateral view) at 50 and 72 h APF. Images are maximum intensity projections of 60 confocal sections. (C) Z-section of an abdomen expressing GFP (green) under control of *pyr-GAL4*, dissected 72 h APF and stained with F-actin dye phalloidin (magenta). GFP-positive cells are the outermost cells and display actin-rich apical trichomes (arrowheads). Nuclei stained with DAPI (blue). (TIF)

S3 Fig. FUCCI monitoring of cell cycle stage in adult fat body precursors and mature adult adipocytes (related to Fig 7). Adult fat body precursors (30 h APF and 60 h APF) and mature adipocytes (2 days after eclosion) expressing FUCCI system of cell cycle monitoring components [33] E2F-GFP (green) and CycB-RFP (magenta) under control of *OK6-GAL4* (precursors) and *Cg-GAL4* (mature adipocytes). In the adult, mature adipocytes are all found in G1 (accumulation of E2F-GFP in absence of CycB-RFP). CycB-RFP separately shown below. (TIF)

S1 Video. Migration of adult fat body precursors into the abdomen.
(MP4)

S2 Video. Proliferation of early adult fat body precursors.
(MP4)

S3 Video. Spreading of adult fat body precursors.
(MP4)

S4 Video. Expression of *htl-GAL4* in adult fat body precursors.
(MP4)

S5 Video. Spreading of *htl^{DN}* and *htl^{CA}* adult fat body precursors.
(MP4)

S6 Video. Detachment of *htl^{DN}* adult fat body precursors.
(MP4)

S7 Video. Fusion of adult fat body precursors.
(MP4)

S1 Table. Detailed genotypes.
(XLSX)

S1 File. Biased random walk model.
(XLSX)

S1 Data. Numerical data.
(XLSX)

Acknowledgments

We thank Deborah Keiko-Hoshizaki for anti-Srp antibody. We also thank the Bloomington *Drosophila* Stock Center (BDSC); Vienna *Drosophila* RNAi Center (VDRC); Tsinghua Fly Center (THFC); Junhai Han, Yulong Li, and Bing Zhou for providing fly strains; and José Martos-Marqués for technical advice on time-lapse imaging.

Author Contributions

Conceptualization: Yuting Lei, Yuwei Huang, José Carlos Pastor-Pareja.

Formal analysis: Yuting Lei, Yuwei Huang, Ke Yang, Xueya Cao, José Carlos Pastor-Pareja.

Funding acquisition: José Carlos Pastor-Pareja.

Investigation: Yuting Lei, Yuwei Huang, Ke Yang, Xueya Cao, Yuzhao Song, Enrique Martín-Blanco, José Carlos Pastor-Pareja.

Resources: Enrique Martín-Blanco.

Supervision: José Carlos Pastor-Pareja.

Visualization: Yuting Lei, Yuwei Huang, Ke Yang, José Carlos Pastor-Pareja.

Writing – original draft: José Carlos Pastor-Pareja.

Writing – review & editing: Yuting Lei, Yuwei Huang, Ke Yang, Xueya Cao, Yuzhao Song, Enrique Martín-Blanco, José Carlos Pastor-Pareja.

References

1. Olzmann JA, Carvalho P. Dynamics and functions of lipid droplets. *Nat Rev Mol Cell Biol.* 2019; 20(3):137–155. <https://doi.org/10.1038/s41580-018-0085-z> PMID: 30523332
2. Le Lièvre CS, Le Douarin NM. Mesenchymal derivatives of the neural crest: analysis of chimaeric quail and chick embryos. *J Embryol Exp Morphol.* 1975; 34(1):125–154. PMID: 1185098
3. Berry DC, Stenesen D, Zeve D, Graff JM. The developmental origins of adipose tissue. *Development.* 2013; 140(19):3939–3949. <https://doi.org/10.1242/dev.080549> PMID: 24046315
4. Spalding KL, Arner E, Westermark PO, Bernard S, Buchholz BA, Bergmann O, et al. Dynamics of fat cell turnover in humans. *Nature.* 2008; 453(7196):783–787. <https://doi.org/10.1038/nature06902> PMID: 18454136
5. Gupta RK. Adipocytes. *Curr Biol.* 2014; 24(20):R988–R993. <https://doi.org/10.1016/j.cub.2014.09.003> PMID: 25442852
6. Brown RJ, Araujo-Vilar D, Cheung PT, Dunger D, Garg A, Jack M, et al. The Diagnosis and Management of Lipodystrophy Syndromes: A Multi-Society Practice Guideline. *J Clin Endocrinol Metab.* 2016; 101(12):4500–4511. <https://doi.org/10.1210/jc.2016-2466> PMID: 27710244
7. Coons LB. *Biology of ticks.* Oxford University Press; 2014.
8. Azpiazu N, Frasch M. tinman and bagpipe: two homeo box genes that determine cell fates in the dorsal mesoderm of *Drosophila*. *Genes Dev.* 1993; 7(7b):1325–1340. <https://doi.org/10.1101/gad.7.7b.1325> PMID: 8101173
9. Riechmann V, Irion U, Wilson R, Grosskortenhaus R, Leptin M. Control of cell fates and segmentation in the *Drosophila* mesoderm. *Development.* 1997; 124(15):2915–2922. <https://doi.org/10.1242/dev.124.15.2915> PMID: 9247334
10. Moore LA, Broihier HT, Van Doren M, Lehmann R. Gonadal mesoderm and fat body initially follow a common developmental path in *Drosophila*. *Development.* 1998; 125(5):837–844. <https://doi.org/10.1242/dev.125.5.837> PMID: 9449666
11. Abel T, Michelson AM, Maniatis T. A *Drosophila* GATA family member that binds to Adh regulatory sequences is expressed in the developing fat body. *Development.* 1993; 119(3):623–633. <https://doi.org/10.1242/dev.119.3.623> PMID: 8187633
12. Sam S, Leise W, Keiko HD. The serpent gene is necessary for progression through the early stages of fat-body development. *Mech Dev.* 1996; 60(2):197–205. [https://doi.org/10.1016/s0925-4773\(96\)00615-6](https://doi.org/10.1016/s0925-4773(96)00615-6) PMID: 9025072
13. Britton JS, Edgar BA. Environmental control of the cell cycle in *Drosophila*: nutrition activates mitotic and endoreplicative cells by distinct mechanisms. *Development.* 1998; 125(11):2149–2158. <https://doi.org/10.1242/dev.125.11.2149> PMID: 9570778
14. Nelliot A, Bond N, Hoshizaki DK. Fat-body remodeling in *Drosophila melanogaster*. *Genesis.* 2006; 44(8):396–400. <https://doi.org/10.1002/dvg.20229> PMID: 16868920
15. Jia Q, Liu Y, Liu H, Li S. Mmp1 and Mmp2 cooperatively induce *Drosophila* fat body cell dissociation with distinct roles. *Sci Rep.* 2014; 4(1):7535. <https://doi.org/10.1038/srep07535> PMID: 25520167

16. Li S, Yu X, Feng Q. Fat Body Biology in the Last Decade. *Annu Rev Entomol.* 2019; 64(1):315–333. <https://doi.org/10.1146/annurev-ento-011118-112007> PMID: 30312553
17. Parra-Peralbo E, Talamillo A, Barrio R. Origin and Development of the Adipose Tissue, a Key Organ in Physiology and Disease. *Front Cell Dev Biol.* 2021; 9:786129.
18. Hoshizaki DK, Lunz R, W Johnson, M Ghosh. Identification of fat-cell enhancer activity in *Drosophila melanogaster* using P-element enhancer traps. *Genome.* 1995; 38(3):497–506. <https://doi.org/10.1139/g95-065> PMID: 7557362
19. Lawrence PA, Johnston P. Observations on cell lineage of internal organs of *Drosophila*. *Development.* 1986; 91(1):251–266. PMID: 3711788
20. Larsen WJ. Cell remodeling in the fat body of an insect. *Tissue Cell.* 1976; 8(1):73–92. Epub 1976/01/01. doi: [https://doi.org/10.1016/0040-8166\(76\)90021-5](https://doi.org/10.1016/0040-8166(76)90021-5) PMID: 178069
21. Haunerland NH, Shirk PD. Regional and Functional Differentiation in the Insect Fat Body. *Annu Rev Entomol.* 1995; 40(1):121–145.
22. Sanyal S. Genomic mapping and expression patterns of C380, OK6 and D42 enhancer trap lines in the larval nervous system of *Drosophila*. *Gene Expr Patterns.* 2009; 9(5):371–380. <https://doi.org/10.1016/j.gep.2009.01.002> PMID: 19602393
23. Rehorn KP, Thelen H, Michelson AM, Reuter R. A molecular aspect of hematopoiesis and endoderm development common to vertebrates and *Drosophila*. *Development.* 1996; 122(12):4023–4031. <https://doi.org/10.1242/dev.122.12.4023> PMID: 9012522
24. Ninov N, Martín-Blanco E. Live imaging of epidermal morphogenesis during the development of the adult abdominal epidermis of *Drosophila*. *Nat Protoc.* 2007; 2(12):3074–3080. <https://doi.org/10.1038/nprot.2007.417> PMID: 18079706
25. Leptin M, Grunewald B. Cell shape changes during gastrulation in *Drosophila*. *Development.* 1990; 110(1):73–84. <https://doi.org/10.1242/dev.110.1.73> PMID: 2081472
26. Gisselbrecht S, Skeath JB, Doe CQ, Michelson AM. *heartless* encodes a fibroblast growth factor receptor (DFR1/DFGF-R2) involved in the directional migration of early mesodermal cells in the *Drosophila* embryo. *Genes Dev.* 1996; 10(23):3003–3017. <https://doi.org/10.1101/gad.10.23.3003> PMID: 8957001
27. Beiman M, Shilo BZ, Volk T. *Heartless*, a *Drosophila* FGF receptor homolog, is essential for cell migration and establishment of several mesodermal lineages. *Genes Dev.* 1996; 10(23):2993–3002. <https://doi.org/10.1101/gad.10.23.2993> PMID: 8957000
28. Gryzik T, Müller HAJ. FGF8-like1 and FGF8-like2 Encode Putative Ligands of the FGF Receptor Htl and Are Required for Mesoderm Migration in the *Drosophila* Gastrula. *Curr Biol.* 2004; 14(8):659–667. <https://doi.org/10.1016/j.cub.2004.03.058> PMID: 15084280
29. Stathopoulos A, Tam B, Ronshaugen M, Frasch M, Levine M. *pyramus* and *thisbe*: FGF genes that pattern the mesoderm of *Drosophila* embryos. *Genes Dev.* 2004; 18(6):687–699. doi: <https://doi.org/10.1101/gad.1166404> PMID: 15075295
30. Doane WW. Developmental physiology of the mutant female sterile(2)adipose of *Drosophila melanogaster*. I. Adult morphology, longevity, egg production, and egg lethality. *J Exp Zool.* 1960; 145(1):1–21. <https://doi.org/10.1002/jez.1401450102> PMID: 13723227
31. Guidotti JE, Br gerie O, Robert A, Debey P, Brechet C, Desdouets C. Liver cell polyploidization: a pivotal role for binuclear hepatocytes. *J Biol Chem.* 2003; 278(21):19095–19101. <https://doi.org/10.1074/jbc.M300982200> PMID: 12626502
32. Sun T, Song Y, Dai J, Mao D, Ma M, Ni JQ, et al. Spectraplakins Maintain Perinuclear Microtubule Organization in *Drosophila* Polyploid Cells. *Dev Cell.* 2019; 49(5):731–47 e7. <https://doi.org/10.1016/j.devcel.2019.03.027> PMID: 31006649
33. Zielke N, Korzelius J, van Straaten M, Bender K, Schuhknecht Gregor FP, Dutta D, et al. Fly-FUCCI: A Versatile Tool for Studying Cell Proliferation in Complex Tissues. *Cell Rep.* 2014; 7(2):588–598. <https://doi.org/10.1016/j.celrep.2014.03.020> PMID: 24726363
34. Makki R, Cinnamon E, Gould AP. The Development and Functions of Oenocytes. *Annu Rev Entomol.* 2014; 59(1):405–425. <https://doi.org/10.1146/annurev-ento-011613-162056> PMID: 24397521
35. Sun J, Macabenta F, Akos Z, Stathopoulos A. Collective Migrations of *Drosophila* Embryonic Trunk and Caudal Mesoderm-Derived Muscle Precursor Cells. *Genetics.* 2020; 215(2):297–322. <https://doi.org/10.1534/genetics.120.303258> PMID: 32487692
36. McMahon A, Supatto W, Fraser SE, Stathopoulos A. Dynamic analyses of *Drosophila* gastrulation provide insights into collective cell migration. *Science.* 2008; 322(5907):1546–1550. <https://doi.org/10.1126/science.1167094> PMID: 19056986
37. Yuan D, Nakanishi N, Jacobs DK, Hartenstein V. Embryonic development and metamorphosis of the scyphozoan *Aurelia*. *Dev Genes Evol.* 2008; 218(10):525–539. <https://doi.org/10.1007/s00427-008-0254-8> PMID: 18850238

38. Pastor-Pareja JC, Grawe F, Martín-Blanco E, García-Bellido A. Invasive cell behavior during *Drosophila* imaginal disc eversion is mediated by the JNK signaling cascade. *Dev Cell*. 2004; 7(3):387–399. <https://doi.org/10.1016/j.devcel.2004.07.022> PMID: 15363413
39. Martín-Blanco E, Gampel A, Ring J, Virdee K, Kirov N, Tolkovsky AM, et al. puckered encodes a phosphatase that mediates a feedback loop regulating JNK activity during dorsal closure in *Drosophila*. *Genes Dev*. 1998; 12(4):557–570. <https://doi.org/10.1101/gad.12.4.557> PMID: 9472024
40. Kalinka AT, Varga KM, Gerrard DT, Preibisch S, Corcoran DL, Jarrells J, et al. Gene expression divergence recapitulates the developmental hourglass model. *Nature*. 2010; 468(7325):811–814. <https://doi.org/10.1038/nature09634> PMID: 21150996
41. Artieri CG, Singh RS. Molecular evidence for increased regulatory conservation during metamorphosis, and against deleterious cascading effects of hybrid breakdown in *Drosophila*. *BMC Biol*. 2010; 8(1):26. <https://doi.org/10.1186/1741-7007-8-26> PMID: 20356354
42. Muha V, Müller H-AJ. Functions and Mechanisms of Fibroblast Growth Factor (FGF) Signalling in *Drosophila melanogaster*. *Int J Mol Sci*. 2013; 14(3):5920–5937. <https://doi.org/10.3390/ijms14035920> PMID: 23493057
43. Davis JR, Huang CY, Zanet J, Harrison S, Rosten E, Cox S, et al. Emergence of embryonic pattern through contact inhibition of locomotion. *Development*. 2012; 139(24):4555–4560. Epub 2012/11/23. <https://doi.org/10.1242/dev.082248> PMID: 23172914
44. Sun J, Stathopoulos A. FGF controls epithelial-mesenchymal transitions during gastrulation by regulating cell division and apicobasal polarity. *Development*. 2018; 145(19). <https://doi.org/10.1242/dev.161927> PMID: 30190277
45. Wu B, Li J, Chou Y-H, Luginbuhl D, Luo L. Fibroblast growth factor signaling instructs ensheathing glia wrapping of *Drosophila* olfactory glomeruli. *Proc Natl Acad Sci U S A*. 2017; 114(29):7505–7512.
46. Chen F, Barkett M, Ram KT, Quintanilla A, Hariharan IK. Biological characterization of *Drosophila* Rapgap1, a GTPase activating protein for Rap1. *Proc Natl Acad Sci U S A*. 1997; 94(23):12485–12490. Epub 1997/11/14. <https://doi.org/10.1073/pnas.94.23.12485> PMID: 9356476
47. Everetts NJ, Worley MI, Yasutomi R, Yosef N, Hariharan IK. Single-cell transcriptomics of the *Drosophila* wing disc reveals instructive epithelium-to-myoblast interactions. *Elife*. 2021; 10:e61276. <https://doi.org/10.7554/eLife.61276> PMID: 33749594
48. Vishal K, Lovato TL, Bragg C, Chechenova MB, Cripps RM. FGF signaling promotes myoblast proliferation through activation of wingless signaling. *Dev Biol*. 2020; 464(1):1–10. <https://doi.org/10.1016/j.ydbio.2020.05.009> PMID: 32445643
49. Dutta D, Shaw S, Maqbool T, Pandya H, Vijayraghavan K. *Drosophila* Heartless acts with Heartbroken/Dof in muscle founder differentiation. *PLoS Biol*. 2005; 3(10):e337. <https://doi.org/10.1371/journal.pbio.0030337> PMID: 16207075
50. Lee DM, Chen EH. *Drosophila* Myoblast Fusion: Invasion and Resistance for the Ultimate Union. *Annu Rev Genet*. 2019; 53(1):67–91. <https://doi.org/10.1146/annurev-genet-120116-024603> PMID: 31283358
51. Toyoda H, Bregerie O, Vallet A, Nalpas B, Pivert G, Brechot C, et al. Changes to hepatocyte ploidy and binuclearity profiles during human chronic viral hepatitis. *Gut*. 2005; 54(2):297–302. <https://doi.org/10.1136/gut.2004.043893> PMID: 15647198
52. Orr-Weaver TL. When bigger is better: the role of polyploidy in organogenesis. *Trends Genet*. 2015; 31(6):307–315. Epub 2015/04/30. <https://doi.org/10.1016/j.tig.2015.03.011> PMID: 25921783
53. Pandit SK, Westendorp B, de Bruin A. Physiological significance of polyploidization in mammalian cells. *Trends Cell Biol*. 2013; 23(11):556–566. <https://doi.org/10.1016/j.tcb.2013.06.002> PMID: 23849927
54. Johnson MB, Butterworth FM. Maturation and aging of adult fat body and oenocytes in *Drosophila* as revealed by light microscopic morphometry. *J Morphol*. 1985; 184(1):51–59. <https://doi.org/10.1002/jmor.1051840106> PMID: 3921720
55. Aguila JR, Hoshizaki DK, Gibbs AG. Contribution of larval nutrition to adult reproduction in *Drosophila melanogaster*. *J Exp Biol*. 2013; 216(3):399–406. <https://doi.org/10.1242/jeb.078311> PMID: 23038728
56. Ito K, Awano W, Suzuki K, Hiromi Y, Yamamoto D. The *Drosophila* mushroom body is a quadruple structure of clonal units each of which contains a virtually identical set of neurones and glial cells. *Development*. 1997; 124(4):761–771. <https://doi.org/10.1242/dev.124.4.761> PMID: 9043058
57. Xu T, Rubin GM. Analysis of genetic mosaics in developing and adult *Drosophila* tissues. *Development*. 1993; 117(4):1223–1237. <https://doi.org/10.1242/dev.117.4.1223> PMID: 8404527